Stochastic dynamics in a time-delayed model for autoimmunity

Article (Accepted Version)

Stochastic dynamics in a time-delayed model for autoimmunity

F. Fatehi[1], Y.N. Kyrychko[2], K.B. Blyuss[2*]

[1] Department of Mathematics, University of York, York, YO10 5DD, UK

[2] Department of Mathematics, University of Sussex, Falmer, Brighton, BN1 9QH, UK

March 27, 2020

Abstract

In this paper we study interactions between stochasticity and time delays in the dynamics of immune response to viral infections, with particular interest in the onset and development of autoimmune response. Starting with a deterministic time-delayed model of immune response to infection, which includes cytokines and T cells with different activation thresholds, we derive an exact delayed chemical master equation for the probability density. We use system size expansion and linear noise approximation to explore how variance and coherence of stochastic oscillations depend on parameters, and to show that stochastic oscillations become more regular when regulatory T cells become more effective at clearing autoreactive T cells. Reformulating the model as an Itô stochastic delay differential equation, we perform numerical simulations to illustrate the dynamics of the model and associated probability distributions in different parameter regimes. The results suggest that even in cases where the deterministic model has stable steady states, in individual stochastic realisations, the model can exhibit sustained stochastic oscillations, whose variance increases as one gets closer to the deterministic stability boundary. Furthermore, in the regime of bi-stability, whereas deterministically the system would approach one of the steady states (or periodic solutions) depending on the initial conditions, due to the presence of stochasticity, it is now possible for the system to reach both of those dynamical states with certain probability. Biological significance of this result lies in highlighting the fact that since normally in a laboratory or clinical setting one would observe a single individual realisation of the course of the disease, even for all parameters characterising the immune system and the strength of infection being the same, there is a proportion of cases where a spontaneous recovery can be observed, and similarly, where a disease can develop in a situation that otherwise would result in a normal disease clearance.

1 Introduction

A functioning immune system is characterised by its ability to effectively recognise and then successfully destroy cells infected by foreign pathogens. This can only be achieved, provided the immune system has the property of *self-tolerance*, which means that it is able to robustly distinguish healthy cells from infected cells by discriminating between self- and foreign antigens expressed on the cell surface [1]. *Autoimmunity* is a condition that is associated with the breakdown of self-tolerance, and it is known to cause debilitating, often life-long diseases, such as type-1 diabetes mellitus, multiple sclerosis, rheumatoid arthritis, and systemic lupus erythematosus (SLE) [2].

Due to the complexity of interactions between different branches of the immune system, it is often very difficult to identify one specific cause for the onset of autoimmune disease in a particular patient, as it is usually a combination of a number of factors, including genetic predisposition, previous exposure to pathogens, age, gender and many others [3, 4, 5, 6]. In light of a prominent role often played by pathogenic infections in the onset and progress of autoimmunity, several mechanisms have been identified that explain pathogen-induced autoimmunity. One of them is *molecular mimicry*, where immune response against an infection can lead to a breakdown of immune tolerance due to cross-reaction with one or more self-antigens that share some of their immunological characteristics with a pathogen [7, 8]. This is particularly relevant for autoimmune diseases associated with viral infections, such as Coxsackie virus for type-1 diabetes [9], and Epstein-Barr virus for multiple sclerosis [2, 10, 11]. Other possible mechanisms of pathogen-induced autoimmunity are *bystander activation*, where T cells specific for an antigen X are activated during immune response against antigen Y as mediated by cytokines [12], *epitope spreading*, where self-antigens released either as a result of direct lysis of self-tissue due to a persisting pathogen, or as part of immune response to a persisting pathogen, result in a secondary immune response against self-antigens, and

*Corresponding author: K.Blyuss@sussex.ac.uk

cryptic antigens that are normally not recognised by the immune system, but as a result of the inflammatory environment following an infection, there can be an increase in protease production and differential processing of released self-epitopes by antigen presenting cells [8]. Very recent murine and human experiments have shown how a single gut bacterium can trigger autoimmune disease in different organs by migrating into them [13]. This lends further credence to the importance of pathogens in mediating autoimmune dynamics.

A number of mathematical models have looked at various aspects of immune dynamics, and in particular, at onset and development of autoimmune response. They have investigated interactions between effector and regulatory T cells (Tregs) [14, 15, 16], the role of T cells in coordinating an effective immune response [17, 18, 19, 20], control of autoimmunity through suppression by Tregs [21], the role of interleukin-2 (IL-2) in mediating T cell interactions [22, 23, 24, 25], and the effects of viral population and the growth function of susceptible host cells on the dynamics of immune response [26, 27]. Grossman et al. [28, 29, 30] proposed an alternative framework of so-called *tunable activation thresholds* (TAT) for modelling the behaviour of T cells in the context of autoimmunity. This approach assumes that the same T cells can perform different immune functions, and they can also adjust their response to stimulation by autoantigens, and this idea that activation of T cells can change during their circulation has been confirmed in murine and human experiments [31, 32, 33, 34]. The importance of tuning lies in the fact that it provides an effective mechanism for improving sensitivity and specificity of T cell signalling in a noisy environment [35, 36], and Scherer et al. [37] and van den Berg and Rand [38] developed and analysed stochastic models for the tuning of activation thresholds.

In the context of autoimmunity arising through a mechanism of molecular mimicry, Blyuss and Nicholson [39, 40] developed a mathematical model of immune response to a viral infection with accounting for T cells with tunable activation thresholds. This model has demonstrated how depending on parameter values, the system can exhibit either normal viral clearance, a sustained chronic infection, or endogenous periodic oscillations that can be interpreted as periods of relapses and remissions often observed in clinical manifestations of autoimmune diseases [41, 42, 43]. These periodic oscillations, however, could only be exhibited by the model, provided the viral population and the population of infected cells are positive, which does not correspond to clinical observations, which rather suggest that progression to an autoimmune disease occurs after the initial viral infection has been fully cleared by the immune system. To overcome this limitation, Fatehi et al. [44] put forward a more realistic version of the same model, which also includes IL-2 and regulatory T cells. This modified model was able to capture all of the above-mentioned dynamical regimes, as well as oscillations in the numbers of autoreactive T cells following clearance of infection. Importantly, this model also exhibited a regime of bi-stability between a disease-free steady state and periodic oscillations corresponding to autoimmune response, suggesting a clinically important observation that it is not only the parameters of the immune system, but also the initial level of infection and the state of the immune system that determine ultimate outcome of the immune response. To account for the intrinsically stochastic nature of many aspects of the immune response [45], Fatehi et al. [46] have explored the effects of stochasticity on the dynamics of immune response in the model and determined for the same parameter regions probability distribution of different immune outcomes. This has also provided practically important insights into how variance of stochastic oscillations depends on different parameters, which is very important for comparison with clinical observations of individual realisations of progression of autoimmune disease. A complementary analysis has been performed by Fatehi et al. [47, 48] to investigate the role played by time delays associated with different aspects of immune response and virus cycle dynamics.

Since both stochasticity and time delays are essential features of the immune system, it is important to consider how their interactions affect immune dynamics. One of the first computational approaches to modelling stochastic systems with time delays was proposed by Bratsun et al. [49] in the context of modelling gene regulation. Subsequently, a number of other delay stochastic simulation algorithms (DSSAs) were proposed, such as 'rejection method' [50], next reaction method [51], 'direct algorithm' [52]. An important point about these more advanced method is that they are able to effectively simulate two types of delayed reactions, namely, *non-consuming delayed reactions* where the reactants of an unfinished reaction can participate in another reaction, as well as *consuming delayed reactions* where the reactants of an unfinished reaction cannot participate in a new reaction. This distinction proved important in models of gene regulatory networks, but applies to a wider range of stochastic delayed models. Besides DSSAs, another approach to analysis of stochastic delayed systems is based on the Delay Chemical Master Equations (DCME) that describe the exact probability distribution of finding the system in a particular state [49, 50]. Leier and Marquez-Lago [53] have presented the most general formulation of DCMEs, which allows one to consider both consuming and non-consuming delayed reactions, and for simple reaction schemes it proved possible to obtain closed form solutions of the DCME. In most cases, however, solving DCME analytically is impossible, while DSSAs are computationally demanding [54, 55], and in

such cases one case use stochastic delay differential equations (SDDEs) to obtain good approximations of probability distributions in stochastic delayed model, which can be obtained in a much more computationally efficient manner. Tian et al. [54] have developed a method for deriving SDDEs directly from DCME models, and showed how these SDDEs can be solved using the Euler-Maruyama method for discrete, as well as distributed time delays. As an alternative, Niu et al. [56, 57] have introduced a strong predictor-corrector method for the numerical solution of SDDEs. Fatehi et al. [58] have recently proposed a new method for deriving SDDE models from DCMEs, which significantly reduces computational complexity.

In this paper, we focus on a fundamental question of how interaction of stochasticity with time delays affects the dynamics of immune response and autoimmunity. Due to a significant role played by the cytokines in mediating the proliferation of T cells during immune response, we will pay particular attention to the time delay associated with this process. As a first step, in the next Section we will briefly review a time-delayed deterministic model of immune response, summarising main biological assumptions, as well discussing conditions for stability of various steady states. In Section 3, we will use this deterministic model as a foundation to derive a delay chemical master equation (DCME) that exactly describes the probability density function of the model, when all cell compartment are represented by discrete random variables. In Section 4, we will develop a system-size expansion of this DCME to obtain a linear-noise approximation (LNA) for fluctuations around deterministic trajectories. This will allow us to determine the magnitude of stochastic fluctuations, as well as the coherence of stochastic oscillations around deterministically stable steady states depends on parameters. Section 5 contains a derivation of an equivalent Itô SDDE model from the DCME, which will then be used in Section 6 for numerical simulations. The paper concludes in Section 7 with a discussion of results and open questions.

2 Deterministic model

In order to understand how stochasticity interacts with time-delayed effects in immune dynamics, we use a model proposed recently by Fatehi et al. [48] to study the dynamics of immune response to viral infection, which is illustrated in Fig. 1. In this model, $A(t)$ denotes a population of healthy host cells that is assumed to grow logistically with a linear growth s and a carrying capacity N. These cells become infected at rate β and move to the compartment $F(t)$ of infected cells. In agreement with other models of viral dynamics [59, 60, 61], it is assumed that infected cells cannot themselves proliferate due to infection, which takes over their cellular machinery for the purpose of producing new virus particles that are subsequently released from such cells upon their lysis. It is, however, possible to make a straightforward modification of our model that would allow infected cells to also reproduce logistically in a manner similar to healthy cells [62, 63]. Unlike an earlier model in [48], we do not explicitly model the population of free virus particles, but instead include a time delay τ_1 to represent the viral lag phase [64], as well as the actual process of infection. In principle, one could also include in the infection term $\beta A(t-\tau_1)F(t-\tau_1)$ an additional factor $e^{-m\tau_1}$ to represent the fraction of already infected cells that survive during the lag period, where m is the death rate of cells that are already infectious but are not yet producing new virions. This was proposed by Herz et al. [65], and subsequently used in a number of other models of virus dynamics [66, 67, 68]. However, to simplify the model we will assume that m is sufficiently small, so that this factor does not have to be explicitly included, as has been effectively done in a number of virus models [69, 70, 71].

In terms of immune response, due to the major role played by T cells in autoimmune dynamics, we focus primarily on their dynamics and do not include B cells, since autoimmune response can develop even in their absence [72]. It is known that stimulation of naïve T cells by antigens results in their proliferation and differentiation into activated T cells that then migrate to the infected tissue [1]. Following activation, T cells that bear $CD8^+$ receptors would become cytotoxic T cells able to destroy infected cells by triggering their apoptosis. Similarly, T cells with $CD4^+$ receptors would become helper T cells [1], some of which, $CD4^+CD25^+$ T cells, are regulatory T cells that perform a very important role of suppressing autoreactive T cells [73, 74]. In order to model autoimmunity arising from a failure of self/non-self discrimination in the immune response, we consider four distinct populations of T cells, naïve/inactive T cells $T_{in}(t)$, $CD4^+CD25^+$ regulatory T cells $T_{reg}(t)$, and two populations of activated $CD8^+$ T cells, namely, normal activated T cells $T_{nor}(t)$, and autoreactive T cells $T_{aut}(t)$. The distinction between normal activated and autoreactive T cells is that the autoreactive T cells have a lower activation threshold, and, as a result of cross-reactivity between some of the epitopes in foreign and self-antigens, they destroy not only infected cells, but also the healthy host cells. Since normal activated T cells are specific to recognising infected cells only, they will be assumed not to be removed or affected by the regulatory T cells. It is assumed that both inactive and regulatory T cells are maintained in a homeostasis, i.e. at some steady levels, in the absence of infection [75]. There are a number of mechanisms involved in this

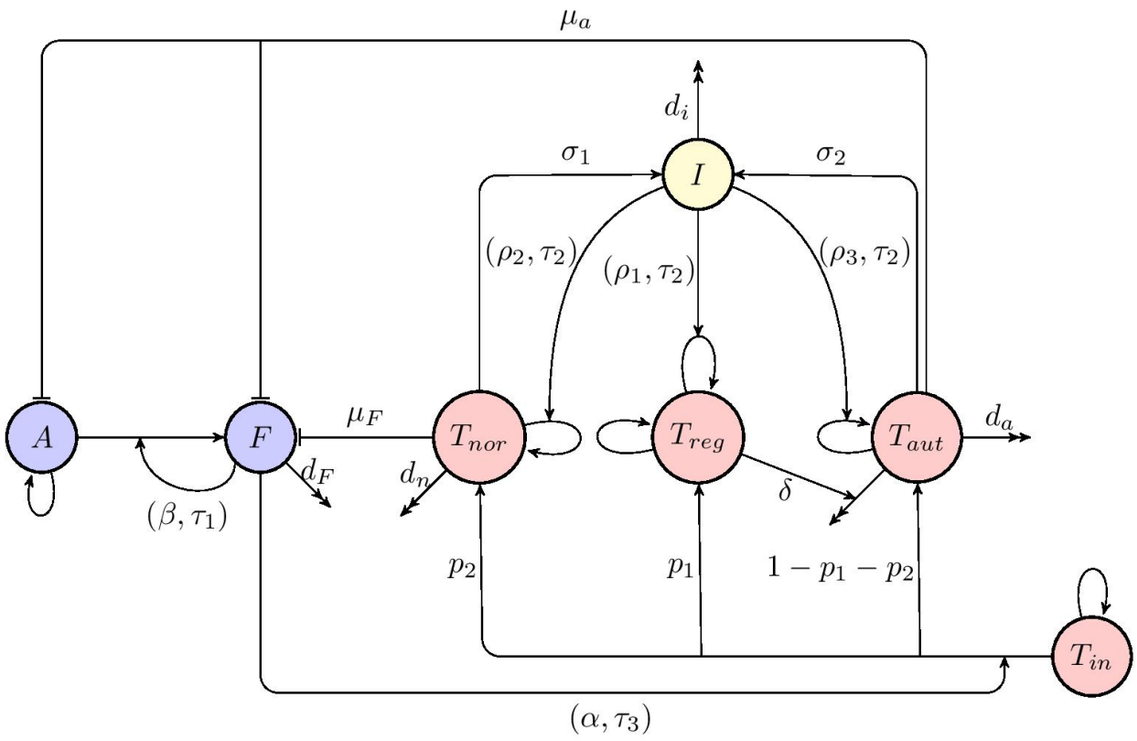

Figure 1: A diagram of immune response to an infection. Blue circles indicate host cells (uninfected and infected cells), red circles denote different T cells (naïve, regulatory, normal activated, and autoreactive T cells), yellow circle show cytokines (interleukin-2). τ_i's inside each of the subnetworks indicate the time delay in the respective processes. Curves with single arrows or bars indicate, respectively, up-regulation or down-regulation. Lines with double arrows indicate natural clearance/death.

process, including post-thymic tuning of T cell receptors and anti-apoptotic signals from cytokines, such as IL-7 and IL-15 in the case of $CD8^+$ cytotoxic T cells [76, 77, 78], and IL-2 in the case of $CD4^+$ regulatory T cells [79, 80]. Iwami et al. [26, 27] have earlier noted that a functional form of the term representing homeostasis can also play a role in determining the dynamics of immune response, and for both naïve and regulatory T cells we choose this function in the form of a constant production, as well as constant degradation rate. Once the cells become infected and recognised as such by the immune system, naïve T cells expand and differentiate, and it is assumed that after some time delay τ_3 a proportion p_1 of them differentiate into further regulatory T cells, a proportion p_2 become normal activated T cells $T_{nor}(t)$, and the remaining proportion $(1 - p_1 - p_2)$ become autoreactive T cells $T_{aut}(t)$. Choosing $p_1 = 0$ would mean that T_{in} only contains the pool of inactive $CD8^+$ cytotoxic T cells (CTLs), from which T_{nor} and T_{aut} are produced through activation, while regulatory T cells are maintained by a separate mechanism. The model also includes a cytokine interleukin-2 (IL-2), which is known to enhance the proliferation of all types of T cells, though it is only secreted by the cytotoxic T cells, and not by the regulatory T cells [1, 81]. Hence, in the model we consider that proliferation of T cells T_{reg}, T_{nor} and T_{aut} is enhanced by IL-2 $I(t)$ at rates ρ_1, ρ_2 and ρ_3, respectively, and this process is characterised by a time delay τ_2, while IL-2 is produced by T_{nor} and T_{aut} at rates σ_1 and σ_2. While regulatory T cells may block the expression of IL-2 by T cells by suppressing IL-2 mRNA, thus restricting T cell proliferation [82, 83, 84], similarly to other studies that analysed the role of IL-2 in T cell dynamics [85, 86, 87], we do not explicitly include this mechanism in our model not to increase its complexity. This effect can, however, be included as an additional term $(-\gamma T_{reg} I)$ in the equation for IL-2 [24, 25], though our earlier analysis of an analogous model has shown that this effect may be smaller compared to other contributions, such as the suppressive effect of regulatory T cells on autoreactive T cells [47].

With these assumptions, the model has the form

$$\frac{dA}{dt} = sA\left(1-\frac{A}{N}\right) - \beta AF - \mu_a T_{aut} A,$$

$$\frac{dF}{dt} = \beta A(t-\tau_1)F(t-\tau_1) - d_F F - \mu_F T_{nor} F - \mu_a T_{aut} F,$$

$$\frac{dT_{in}}{dt} = \lambda_{in} - d_{in} T_{in} - \alpha T_{in} F,$$

$$\frac{dT_{reg}}{dt} = \lambda_r - d_r T_{reg} + p_1 \alpha T_{in}(t-\tau_3)F(t-\tau_3) + \rho_1 I(t-\tau_2)T_{reg}(t-\tau_2), \tag{1}$$

$$\frac{dT_{nor}}{dt} = p_2 \alpha T_{in}(t-\tau_3)F(t-\tau_3) - d_n T_{nor} + \rho_2 I(t-\tau_2)T_{nor}(t-\tau_2),$$

$$\frac{dT_{aut}}{dt} = (1-p_1-p_2)\alpha T_{in}(t-\tau_3)F(t-\tau_3) - d_a T_{aut} - \delta T_{reg} T_{aut} + \rho_3 I(t-\tau_2)T_{aut}(t-\tau_2),$$

$$\frac{dI}{dt} = \sigma_1 T_{nor} + \sigma_2 T_{aut} - d_i I.$$

This model has been analysed earlier in Fatehi et al. [47, 48], who have shown that it has at most four biologically feasible steady states. The first one, a *disease-free steady state*, is given by

$$S_1^* = \left(N, 0, \frac{\lambda_{in}}{d_{in}}, \frac{\lambda_r}{d_r}, 0, 0, 0\right),$$

and it is stable if $d_F > \beta N$ and unstable if $d_F < \beta N$, irrespective of the values of time delays. The second and third steady states can be found as

$$S_2^* = \left(0, 0, \frac{\lambda_{in}}{d_{in}}, x_4^*, 0, \frac{d_i\left(d_a+\delta x_4^*\right)}{\rho_3\sigma_2}, \frac{d_a+\delta x_4^*}{\rho_3}\right),$$

and

$$S_3^* = \left(\frac{N\left[\rho_3\sigma_2 s - \mu_a d_i\left(d_a+\delta x_4^*\right)\right]}{\rho_3\sigma_2 s}, 0, \frac{\lambda_{in}}{d_{in}}, x_4^*, 0, \frac{d_i\left(d_a+\delta x_4^*\right)}{\rho_3\sigma_2}, \frac{d_a+\delta x_4^*}{\rho_3}\right),$$

where x_4^* satisfies the following quadratic equation

$$\rho_1\delta\left(x_4^*\right)^2 + \left(\rho_1 d_a - \rho_3 d_r\right)x_4^* + \rho_3\lambda_r = 0. \tag{2}$$

These steady states are stable, provided

$$\frac{s\sigma_2}{\mu_a d_i}K < \frac{d_a+\delta x_4^*}{\rho_3} < \frac{d_n}{\rho_2},$$

where $K = 1$ for S_2^*, and $K = (\beta N - d_F)/(s+\beta N)$ for S_3^*, and the following equation

$$\Delta(\tau_2, \lambda) = p_2(\lambda)e^{-2\lambda\tau_2} + p_1(\lambda)e^{-\lambda\tau_2} + p_0(\lambda) = 0, \tag{3}$$

where

$$\begin{aligned}
p_2(\lambda) =& \frac{\rho_1\left(d_a+\delta x_4^*\right)^2}{\rho_3}\left(\lambda+2d_i\right),\\
p_1(\lambda) =& \frac{-\left(d_a+\delta x_4^*\right)}{\rho_3}\Big\{(\rho_1+\rho_3)\lambda^2 + \left[\rho_1\left(d_a+\delta x_4^*\right) + d_i\rho_1 + 2d_i\rho_3 + d_r\rho_3\right]\lambda\\
&+ d_i(\rho_1 d_a + 2d_r\rho_3)\Big\},\\
p_0(\lambda) =& \lambda^3 + \left(d_i + d_r + d_a + \delta x_4^*\right)\lambda^2 + \left[d_i\left(d_a+\delta x_4^*\right) + d_r\left(d_a+\delta x_4^*\right) + d_i d_r\right]\lambda\\
&+ d_i d_r\left(d_a+\delta x_4^*\right),
\end{aligned}$$

only has roots with negative real part. Biologically, the steady state S_2^* represents the death of host cells, while S_3^* corresponds to an autoimmune state. Depending on parameters, the steady state S_3^* can lose its stability through a Hopf bifurcation, which occurs when a pair of characteristics roots of equation (3) crosses the imaginary axis. In this case, one would observe periodic oscillations around S_3^* that can be interpreted from immunological perspective as an autoimmune state, characterised by the clearance of the initial infection, followed by sustained endogenous oscillations in the numbers of autoreactive T cells [47, 48, 44]. The final steady state S_4^* has all of its components positive, and it corresponds to the state of chronic infection. Having established conditions for stability of various steady states, we can now consider how the dynamics of the system is influenced by stochasticity, and how the stochasticity interacts with different time delays present in the system.

3 Stochastic model: a delayed chemical master equation

To develop a stochastic version of the model (1), we introduce variables $X_1(t), \ldots, X_7(t) \in \{0, 1, 2, \ldots\}$ as discrete random variables representing, respectively, the numbers of uninfected cells, infected cells, naïve T cells, regulatory T cells, normal activated T cells, autoreactive T cells, and interleukin 2 (IL-2) at time t, with the initial condition $\mathbf{X}(t) = \boldsymbol{\varphi}(t)$ for $t \in [-\tau, 0]$, where $\tau = \max\{\tau_1, \tau_2, \tau_3\}$. It is assumed that all these cells interact within some fixed volume Ω. The state change vector characterising each specific interaction between different cells R_j is denoted by $\mathbf{v}_j$, and its propensity function is given by $a_j(\mathbf{X}(t))$ in any given state $\mathbf{X}(t) = (X_1(t), X_2(t), \ldots, X_7(t))$. The propensity functions corresponding to interactions and transitions illustrated in Fig. 1 are given in the system (12) in **Appendix A**.

As already mentioned in the Introduction, when deriving the *delay chemical master equation* (DCME), one has to carefully account for delayed transitions/interactions. Following an approach proposed by Barrio et al. [50] and subsequently elaborated by Cai [52] for chemical reactions (within our model, individual cell populations can be interpreted and chemical reactants, and interactions between them as reaction), we will divide all reactions into three types: non-delayed reactions, non-consuming delayed reactions, and consuming delayed reactions. The distinction between these three types of reaction lies in when the associated state of the system gets updated, and what the corresponding state change vector is. For non-delayed and non-consuming delayed reactions, there is a single time point where the update of the system state happens both for original reactants and for the resulting products - it happens either immediately in the case of non-delayed reactions, or, respectively, after the end of delay for delayed non-consuming reactions. In contrast, for consuming delayed reactions, there are two distinct update points: original reactants are updated at the initiation of reaction, while the products are updated at the end of time delay. From a biological/chemical point of view, the difference between non-consuming and consuming delayed reactions is that during non-consuming reactions, reactants can also participate in other reactions (hence, the name, as reactants are not "consumed" by the reaction), whereas in consuming reactions, once they start, the reactants are consumed and thus cannot participate in any other reactions until current reactions finish. As an example, gene transcription can be interpreted as non-consuming reactions, since it is possible for a single gene to be simultaneously transcribed by several different RNA polymerases, and moreover, the DNA molecule itself is not consumed by the first transcription, but is rather available for another transcription even before the end of the current one. In contrast, transport of compounds within or outside the cell is a consuming reaction, since the molecules leave one compartment, and after some period of time appear in another compartment, clearly indicating two different updates: one at the start of reaction, and another at the end of delay period.

Based on the deterministic model (1), stimulation and subsequent proliferation of activated T cells with a positive growth signal from IL-2 is a non-consuming delayed reaction. In contrast, activation of inactive T cells, and production of infected cells from uninfected cells are consuming delayed reactions. Therefore, the state change vector for these reactions should be split into two vectors, with one of them indicating the state change in the absence of delays, and the other one showing the state change of products which occurs with a delay [53].

If we denote the probability of finding the system in the state $\mathbf{n} = (n_1, n_2, n_3, n_4, n_5, n_6, n_7)$ with $n_i \in \{0, 1, 2, ...\}$ at time t by

$$P(\mathbf{n}, t) = \text{Prob}\{\mathbf{X}(t) = \mathbf{n} | \boldsymbol{\varphi}(t)\},$$

it then satisfies the following DCME [49, 50, 53]

$$\begin{aligned}
\frac{\partial P(\mathbf{n}, t)}{\partial t} = \Big\{ & (\varepsilon_1^- - 1) a_1(\mathbf{n}) + (\varepsilon_1^+ - 1)\big[a_2(\mathbf{n}) + a_3(\mathbf{n})\big] + (\varepsilon_2^+ - 1) a_4(\mathbf{n}) \\
& + (\varepsilon_3^- - 1) a_5(\mathbf{n}) + (\varepsilon_3^+ - 1)\big[a_6(\mathbf{n}) + a_7(\mathbf{n}) + a_8(\mathbf{n}) + a_9(\mathbf{n})\big] + (\varepsilon_4^- - 1) a_{10}(\mathbf{n}) \\
& + (\varepsilon_4^+ - 1) a_{12}(\mathbf{n}) + (\varepsilon_5^+ - 1) a_{14}(\mathbf{n}) + (\varepsilon_6^+ - 1) a_{16}(\mathbf{n}) + (\varepsilon_7^- - 1) a_{17}(\mathbf{n}) \\
& + (\varepsilon_7^+ - 1) a_{18}(\mathbf{n}) \Big\} P(\mathbf{n}, t) + \sum_{\mathbf{m} \in I(\mathbf{n})} \big[a_3(\mathbf{m}) (\varepsilon_2^- - 1) P(\mathbf{n}, t; \mathbf{m}, t - \tau_1) \big] \\
& + \sum_{\mathbf{m} \in I(\mathbf{n})} \Big[\big\{ a_{11}(\mathbf{m}) (\varepsilon_4^- - 1) + a_{13}(\mathbf{m}) (\varepsilon_5^- - 1) + a_{15}(\mathbf{m}) (\varepsilon_6^- - 1) \big\} P(\mathbf{n}, t; \mathbf{m}, t - \tau_2) \Big] \\
& + \sum_{\mathbf{m} \in I(\mathbf{n})} \Big[\big\{ a_7(\mathbf{m}) (\varepsilon_4^- - 1) + a_8(\mathbf{m}) (\varepsilon_5^- - 1) + a_9(\mathbf{m}) (\varepsilon_6^- - 1) \big\} P(\mathbf{n}, t; \mathbf{m}, t - \tau_3) \Big],
\end{aligned} \tag{4}$$

where $I(\mathbf{n})$ is the set of all possible system states in the past, from which the state $\mathbf{n}$ is able to follow via a chain of transitions, $P(\mathbf{n}, t; \mathbf{m}, t-\tau)$ is the joint probability of finding the system in state $\mathbf{n}$ at time t and in state $\mathbf{m}$ at time $t-\tau$, and shift operators $\varepsilon_i^{\pm}$ are defined as follows,

$$\varepsilon_i^{\pm} f(n_1, n_2, n_3, n_4, n_5, n_6, n_7, t) = f(n_1, ..., n_i \pm 1, ..., n_7, t), \text{ for each } 1 \leq i \leq 7,$$

and if $n_i < 0$ for any $1 \leq i \leq 7$, then $P(\mathbf{n}, t) = 0$.

Since solving this equation analytically is not possible, it can either be simulated numerically using some DSSAs, which is computationally expensive [54, 55, 88], or one can develop some approximations of this equation that can provide both analytical insights and analogous representations that are more computationally efficient.

4 System size expansion and fluctuations

To make analytical progress in the analysis of the DCME (4), we will use the so-called *system size expansion*, or van Kampen's expansion [89] that is often used to construct a continuous approximation for discrete stochastic models [90, 91, 55]. This will allow us to decompose time evolution of each cell population into deterministic and stochastic components, thus providing a methodology for analysis of fluctuations around deterministic attractors [55, 92]. In order to apply system size expansion to the DCME (4), we consider each n_i to be of order Ω, with fluctuations of order $\Omega^{1/2}$, which can be written as follows,

$$n_i(t) = \Omega x_i(t) + \Omega^{1/2} \xi_i(t), \quad i = 1, 2, \ldots, 7,$$

where $x_i(t)$ are determined by the deterministic rate equations, and $\xi_i(t)$ describe random fluctuations around the deterministic solution. Similarly, for delayed variables we write [92]

$$m_i(t-\tau_j) = \Omega x_i(t-\tau_j) + \Omega^{1/2} \eta_i(t), \quad i = 1, \ldots, 7, \ j = 1, 2, 3,$$

where the index j is chosen depending on the delayed reaction being considered. For example, if it is the reaction of production of infected cells from uninfected cells, then $m_i(t-\tau_1) = \Omega x_i(t-\tau_1) + \Omega^{1/2}\eta_i(t), \quad i = 1, 2, \ldots, 7$.

The probability distributions $P(\mathbf{n}, t)$ and $P(\mathbf{n}, t; \mathbf{m}, t-\tau_j)$ can be written as functions of $\boldsymbol{\xi} = (\xi_1, \ldots, \xi_7)^T$ and $\boldsymbol{\eta} = (\eta_1, \ldots, \eta_7)^T$, i.e.

$$\begin{aligned} P(\mathbf{n}, t) &= P(\Omega \mathbf{x} + \Omega^{1/2}\boldsymbol{\xi}, t) = \Pi(\boldsymbol{\xi}, t), \\ P(\mathbf{n}, t; \mathbf{m}, t-\tau_j) &= \Pi(\boldsymbol{\xi}, t; \boldsymbol{\eta}, t-\tau_j), \quad j = 1, 2, 3, \end{aligned}$$

which implies

$$\frac{dP(\mathbf{n}, t)}{dt} = \frac{\partial \Pi}{\partial t} - \sum_{i=1}^{7} \Omega^{1/2} \frac{dx_i}{dt} \frac{\partial \Pi}{\partial \xi_i}. \tag{5}$$

To expand the master equation in a power series in $\Omega^{-1/2}$, we use the following expansions for step operators $\varepsilon_i^{\pm}$

$$\varepsilon_i^{\pm} = 1 \pm \Omega^{-1/2} \frac{\partial}{\partial \xi_i} + \frac{1}{2}\Omega^{-1} \frac{\partial^2}{\partial \xi_i^2} \pm \cdots. \tag{6}$$

with similar expansions for propensity functions a_i, where we also rescale the parameters as follows,

$$\begin{aligned} &d_2 = \frac{s}{N\Omega}, \quad \beta = \frac{\widetilde{\beta}}{\Omega}, \quad \alpha = \frac{\widetilde{\alpha}}{\Omega}, \quad \mu_a = \frac{\widetilde{\mu}_a}{\Omega}, \quad \mu_F = \frac{\widetilde{\mu}_F}{\Omega}, \quad \rho_i = \frac{\widetilde{\rho}_i}{\Omega}, \quad i = 1, 2, 3, \\ &\delta = \frac{\widetilde{\delta}}{\Omega}, \quad \lambda_{in} = \frac{\widetilde{\lambda}_{in}}{\Omega}, \quad \lambda_r = \frac{\widetilde{\lambda}_r}{\Omega}, \end{aligned}$$

and drop tildes for notational convenience. To give two examples, expansions of propensities for non-delayed and non-consuming delayed reactions have the form

$$a_1(\mathbf{n}) = s\xi_1\Omega^{1/2} + sx_1\Omega,$$

and

$$a_7(\mathbf{m}) = p_1\alpha\eta_2\eta_3 + \big(p_1\alpha x_2(t-\tau_3)\eta_3 + p_1\alpha x_3(t-\tau_3)\eta_2\big)\Omega^{1/2} + p_1\alpha x_2(t-\tau_3)x_3(t-\tau_3)\Omega,$$

with the expansions of remaining propensities given in **Appendix B**.

Substituting expressions (5) and (6), together with the expansions for propensity functions, into the DCME (4) shows that the left-hand side of the equation only contains terms of the order $\Omega^{1/2}$ and Ω^0, while the right-hand side has terms of the order $\Omega^{1/2}$, Ω^0, and $\Omega^{-n/2}$, for $n \in \mathbb{N}$, and we

will ignore the terms of order $\Omega^{-n/2}$ [92, 46]. To show how the process of substitution works, let us illustrate expansions for one non-delayed term

$$
\begin{aligned}
(\varepsilon_1^- - 1)a_1(\mathbf{n})P(\mathbf{n},t) &= \left(-\Omega^{-1/2}\frac{\partial}{\partial\xi_1} + \frac{1}{2}\Omega^{-1}\frac{\partial^2}{\partial\xi_1^2}\right)\left[s\xi_1\Omega^{1/2} + sx_1\Omega\right]\Pi(\boldsymbol{\xi},t) \\
&= -sx_1\Omega^{1/2}\frac{\partial\Pi(\boldsymbol{\xi},t)}{\partial\xi_1} - \frac{\partial}{\partial\xi_1}\left[s\xi_1\Pi\right]\Omega^0 + \frac{1}{2}sx_1\frac{\partial^2\Pi(\boldsymbol{\xi},t)}{\partial\xi_1^2}\Omega^0,
\end{aligned}
$$

and one delayed term of the DCME (4)

$$
\begin{aligned}
&\sum_{\mathbf{m}\in I(\mathbf{n})}\left[a_3(\mathbf{m})(\varepsilon_2^- - 1)P(\mathbf{n},t;\mathbf{m},t-\tau_1)\right] = \\
&\int_{\boldsymbol{\eta}}\left(-\Omega^{-1/2}\frac{\partial}{\partial\xi_2} + \frac{1}{2}\Omega^{-1}\frac{\partial^2}{\partial\xi_2^2}\right)\left[\big(\beta x_1(t-\tau_1)\eta_2 + \beta x_2(t-\tau_1)\eta_1\big)\Omega^{1/2} + \beta x_1(t-\tau_1)x_2(t-\tau_1)\Omega\right] \\
&\quad \Pi(\boldsymbol{\xi},t;\boldsymbol{\eta},t-\tau_1)d\boldsymbol{\eta} \\
&= -\beta x_1(t-\tau_1)x_2(t-\tau_1)\Omega^{1/2}\frac{\partial\Pi(\boldsymbol{\xi},t)}{\partial\xi_2} - \frac{\partial}{\partial\xi_2}\int_{\boldsymbol{\eta}}\big(\beta x_1(t-\tau_1)\eta_2 + \beta x_2(t-\tau_1)\eta_1\big)\Pi(\boldsymbol{\xi},t;\boldsymbol{\eta},t-\tau_1)d\boldsymbol{\eta}\Omega^0 \\
&\quad + \frac{1}{2}\beta x_1(t-\tau_1)x_2(t-\tau_1)\frac{\partial^2\Pi(\boldsymbol{\xi},t)}{\partial\xi_2^2}\Omega^0,
\end{aligned}
$$

with all other terms being computed in the same way. After substitution, collecting terms of order $\Omega^{1/2}$ yields system (1) describing macroscopic behaviour of the model.

At the next order, i.e. at order Ω^0, we obtain a linear delayed Fokker-Planck equation, known as the linear noise approximation (LNA), that describes stochastic fluctuations around a deterministic trajectory, as shown in **Appendix C**. Following Phillips et al. [55], we use the structure of this equation to derive a system of equations that describes the delayed Langevin dynamics of fluctuations around any deterministic steady states $S^* = (x_1^*, x_2^*, \ldots, x_7^*)$ of the model (1). This system has the form

$$
\begin{aligned}
\dot{\xi_1} &= (s - 2d_2x_1^* - \beta x_2^* - \mu_a x_6^*)\xi_1 - \beta x_1^*\xi_2 - \mu_a x_1^*\xi_6 + \zeta_1, \\
\dot{\xi_2} &= \beta x_2^*\xi_1(t-\tau_1) + \beta x_1^*\xi_2(t-\tau_1) - (d_F + \mu_F x_5^* + \mu_a x_6^*)\xi_2 - \mu_F x_2^*\xi_5 - \mu_a x_2^*\xi_6 + \zeta_2, \\
\dot{\xi_3} &= -\alpha x_3^*\xi_2 - (d_{in} + \alpha x_2^*)\xi_3 + \zeta_3, \\
\dot{\xi_4} &= -d_r\xi_4 + p_1\alpha x_3^*\xi_2(t-\tau_3) + p_1\alpha x_2^*\xi_3(t-\tau_3) + \rho_1 x_7^*\xi_4(t-\tau_2) + \rho_1 x_4^*\xi_7(t-\tau_2) + \zeta_4, \\
\dot{\xi_5} &= -d_n\xi_5 + p_2\alpha x_3^*\xi_2(t-\tau_3) + p_2\alpha x_2^*\xi_3(t-\tau_3) + \rho_2 x_7^*\xi_5(t-\tau_2) + \rho_2 x_5^*\xi_7(t-\tau_2) + \zeta_5, \\
\dot{\xi_6} &= -\delta x_6^*\xi_4 - (d_a + \delta x_4^*)\xi_6 + (1-p_1-p_2)\alpha x_3^*\xi_2(t-\tau_3) + (1-p_1-p_2)\alpha x_2^*\xi_3(t-\tau_3) \\
&\quad + \rho_3 x_7^*\xi_6(t-\tau_2) + \rho_3 x_6^*\xi_7(t-\tau_2) + \zeta_6, \\
\dot{\xi_7} &= \sigma_1\xi_5 + \sigma_2\xi_6 - d_i\xi_7 + \zeta_7,
\end{aligned}
\tag{7}
$$

where $\boldsymbol{\zeta}(t) = (\zeta_1(t), \zeta_2(t), \ldots, \zeta_7(t))^T$ is a vector of seven independent Gaussian white noise variables with zero mean, and the noise correlators given by

$$
\begin{aligned}
\langle\zeta_1(t)\zeta_1(t')\rangle &= (sx_1^* + d_2{x_1^*}^2 + \beta x_1^*x_2^* + \mu_a x_1^*x_6^*)\delta(t-t'), \\
\langle\zeta_2(t)\zeta_2(t')\rangle &= (\beta x_1^*x_2^* + d_F x_2^* + \mu_F x_2^*x_5^* + \mu_a x_2^*x_6^*)\delta(t-t'), \\
\langle\zeta_3(t)\zeta_3(t')\rangle &= (\lambda_{in} + d_{in}x_3^* + \alpha x_2^*x_3^*)\delta(t-t'), \\
\langle\zeta_4(t)\zeta_4(t')\rangle &= (\lambda_r + d_r x_4^* + p_1\alpha x_2^*x_3^* + \rho_1 x_4^*x_7^*)\delta(t-t'), \\
\langle\zeta_5(t)\zeta_5(t')\rangle &= (p_2\alpha x_2^*x_3^* + d_n x_5^* + \rho_2 x_5^*x_7^*)\delta(t-t'), \\
\langle\zeta_6(t)\zeta_6(t')\rangle &= \big((1-p_1-p_2)\alpha x_2^*x_3^* + d_a x_6^* + \delta x_4^*x_6^* + \rho_3 x_6^*x_7^*\big)\delta(t-t'), \\
\langle\zeta_7(t)\zeta_7(t')\rangle &= (\sigma_1 x_5^* + \sigma_2 x_6^* + d_i x_7^*)\delta(t-t'), \\
\langle\zeta_i(t)\zeta_j(t')\rangle &= 0, \quad \forall\ i \neq j.
\end{aligned}
$$

Using a Fourier transformation of the model (7), one can find the power spectral density (PSD) of the fluctuations, which can be used to determine the variance and coherence of stochastic oscillations. Fourier transform of the model (7) gives

$$
M(\omega)\tilde{\boldsymbol{\xi}}(\omega) = \tilde{\boldsymbol{\zeta}}(\omega),
$$

where $M(\omega) = i\omega I - M_1 - e^{-i\omega\tau_1}M_2 - e^{-i\omega\tau_2}M_3 - e^{-i\omega\tau_3}M_4$, and

$$M_1 = \begin{pmatrix} s - 2d_2x_1^* - \mu_a x_6^* - \beta x_2^* & -\beta x_1^* & 0 & 0 & 0 & -\mu_a x_1^* & 0 \\ 0 & -d_F - \mu_F x_5^* - \mu_a x_6^* & 0 & 0 & -\mu_F x_2^* & \mu_a x_2^* & 0 \\ 0 & -\alpha x_3^* & -d_{in} - \alpha x_2^* & 0 & 0 & 0 & 0 \\ 0 & 0 & 0 & -d_r & 0 & 0 & 0 \\ 0 & 0 & 0 & 0 & -d_n & 0 & 0 \\ 0 & 0 & 0 & -\delta x_6^* & 0 & -d_a - \delta x_4^* & 0 \\ 0 & 0 & 0 & 0 & \sigma_1 & \sigma_2 & -d_i \end{pmatrix},$$

$$(M_2)_{ij} = \begin{cases} \beta x_2^*, & \text{if } (i,j) = (1,2), \\ \beta x_1^*, & \text{if } (i,j) = (2,2), \\ 0, & \text{otherwise,} \end{cases}$$

$$(M_3)_{ij} = \begin{cases} \rho_1 x_7^*, & \text{if } (i,j) = (4,4), \\ \rho_1 x_4^*, & \text{if } (i,j) = (4,7), \\ \rho_2 x_7^*, & \text{if } (i,j) = (5,5), \\ \rho_2 x_5^*, & \text{if } (i,j) = (5,7), \\ \rho_3 x_7^*, & \text{if } (i,j) = (6,6), \\ \rho_3 x_6^*, & \text{if } (i,j) = (6,7), \\ 0, & \text{otherwise,} \end{cases} \quad (M_4)_{ij} = \begin{cases} p_1\alpha x_3^*, & \text{if } (i,j) = (4,2), \\ p_1\alpha x_2^*, & \text{if } (i,j) = (4,3), \\ p_2\alpha x_3^*, & \text{if } (i,j) = (5,2), \\ p_2\alpha x_2^*, & \text{if } (i,j) = (5,3), \\ (1-p_1-p_2)\alpha x_3^*, & \text{if } (i,j) = (6,2), \\ (1-p_1-p_2)\alpha x_2^*, & \text{if } (i,j) = (6,3), \\ 0, & \text{otherwise.} \end{cases}$$

Introducing the matrix of spectra $S(\omega)$ as $S_{ij}(\omega) = \langle \xi_i(\omega)\xi_j(\omega)^\dagger \rangle$ [55], we then have

$$S(\omega) = M(\omega)^{-1} \langle \tilde{\boldsymbol{\zeta}}(\omega)\tilde{\boldsymbol{\zeta}}(\omega)^\dagger \rangle \big(M(\omega)^\dagger\big)^{-1},$$

where

$$\langle \tilde{\boldsymbol{\zeta}}(\omega)\tilde{\boldsymbol{\zeta}}(\omega')^\dagger \rangle = \mathrm{diag}\{b_1, b_2, \ldots, b_7\}\delta(\omega + \omega'),$$

and

$$b_i = \begin{cases} sx_1^* + d_2 x_1^{*2} + \beta x_1^* x_2^* + \mu_a x_1^* x_6^*, & \text{if } i = 1, \\ \beta x_1^* x_2^* + d_F x_2^* + \mu_F x_2^* x_5^* + \mu_a x_2^* x_6^*, & \text{if } i = 2, \\ \lambda_{in} + d_{in} x_3^* + \alpha x_2^* x_3^*, & \text{if } i = 3, \\ \lambda_r + d_r x_4^* + p_1\alpha x_2^* x_3^* + \rho_1 x_4^* x_7^*, & \text{if } i = 4, \\ p_2\alpha x_2^* x_3^* + d_n x_5^* + \rho_2 x_5^* x_7^*, & \text{if } i = 5, \\ (1-p_1-p_2)\alpha x_2^* x_3^* + d_a x_6^* + \delta x_4^* x_6^* + \rho_3 x_6^* x_7^*, & \text{if } i = 6, \\ \sigma_1 x_5^* + \sigma_2 x_6^* + d_i x_7^*, & \text{if } i = 7. \end{cases}$$

Using this approach, it can be easily shown that in the case where the macroscopic model (1) converges to either of the steady states S_2^* or S_3^*, the power spectrum for the number of regulatory T cells ($S_{4,4}(\omega)$), which is denoted as $P_r(\omega)$, is given by

$$P_{reg}(\omega) = \frac{b_4|L|^2 + b_6\sigma_2^2\rho_1^2 x_4^{*2} + b_7\rho_1^2 x_4^{*2}\left|i\omega + d_a + \delta x_4^* - \rho_3 e^{-i\omega\tau_2}x_7^*\right|^2}{|\det(D)|^2}, \tag{8}$$

where $L = (i\omega + d_i)\left(i\omega + d_a + \delta x_4^* - \rho_3 e^{-i\omega\tau_2}x_7^*\right) - \rho_3\sigma_2 e^{-i\omega\tau_2}x_6^*$, and

$$D = \begin{pmatrix} i\omega + d_r - \rho_1 e^{-i\omega\tau_2}x_7^* & 0 & -\rho_1 e^{-i\omega\tau_2}x_4^* \\ \delta x_6^* & i\omega + d_a + \delta x^* - \rho_3 e^{-i\omega\tau_2}x_7^* & -\rho_3 e^{-i\omega\tau_2}x_7^* \\ 0 & -\sigma_2 & i\omega + d_i \end{pmatrix},$$

and the PSDs of other state variables can be obtained in a similar way.

At any steady state, the covariance matrix Ξ with $\Xi_{ij} = \langle \xi_i(t)\xi_j(t)\rangle - \langle \xi_i(t)\rangle\langle \xi_j(t)\rangle = \langle \xi_i(t)\xi_j(t)\rangle$ is independent of time, and is thus given by [93]

$$\Xi = \frac{1}{2\pi}\int_{-\infty}^{+\infty} S(\omega)d\omega = \frac{1}{\pi}\int_{0}^{+\infty} S(\omega)d\omega. \tag{9}$$

To relate the results of this analysis to the outcome of direct numerical simulations of the stochastic model, it is instructive to express the covariance matrix in terms of actual numbers of cells in each compartment, rather than deviations from stationary values. This can be achieved by defining the covariance matrix C as $C_{ij} = \langle (n_i - \langle n_i\rangle)(n_j - \langle n_j\rangle)\rangle$, which is related to Ξ through $C_{ij} = \Omega\Xi_{ij}$

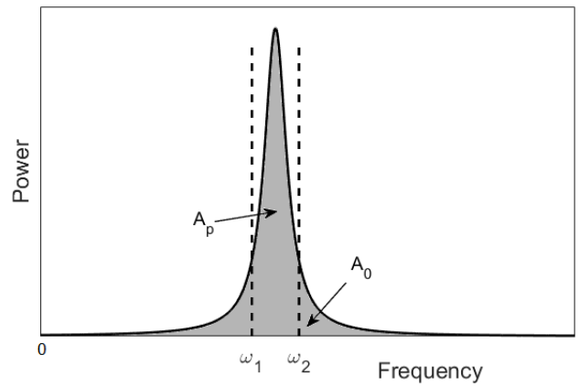

Figure 2: Coherence of stochastic oscillations c defined as the spectral power associated with a range of frequencies around the peak A_p relative to the total area under the PSD curve A_0 [55, 95].

[46]. When there is no delay, as an alternative to numerical computation of matrices Ξ and C by evaluation of the matrix of spectra $S(\omega)$ and its subsequent numerical integration, one could also determine these matrices by solving the corresponding Lyapunov equation [46, 94]. Either of those approaches allows one to compute the value of variance of fluctuations around any steady state of the deterministic model.

In order to quantify how well-structured stochastic oscillations are around the dominant spectral frequency for any of the relevant state variables, we can use the notion of coherence [55, 93, 95]. Choosing a particular state variable $X(t)$, we can consider the power spectral density $P(\omega)$ of stochastic oscillations of this variable around its steady state value X^*. The overall level of fluctuations can be measured by the mean-square variance

$$A_0 = \lim_{T\to\infty} \int_{-T}^{+T} [X(t) - X^*]^2 \, dt = \int_0^{+\infty} 2P(\omega) d\omega.$$

Focusing on the particular interval of frequencies $[\omega_1, \omega_2]$ around the peak frequency in the distribution $P(\omega)$, as shown in Fig. 2, one can compute the quantity

$$A_p = \int_{\omega_1}^{\omega_2} 2P(\omega) d\omega,$$

and then define *coherence of stochastic oscillations* as $c = A_p/A_0$ [55, 95].

5 Itô SDDE model

Using the method presented in [58], we now derive a computationally efficient SDDE model associated with the DCME (4). Let $\mathbf{Y}(t) = (Y_1(t), Y_2(t), Y_3(t), Y_4(t), Y_5(t), Y_6(t), Y_7(t))^T$ be a continuous random vector for the sizes of various cell compartments at time t, and Δt be small enough so that during this time interval at most one change can occur in state variables. These changes together with their probabilities are listed in Table 2 in **Appendix D**. In this table, reactions 3, 7, 8 and 9 that are associated with infection and proliferation of different types of T cells from naïve/inactive T cells are consuming delayed reactions; reactions 11, 13 and 15 describing the delayed impact of IL-2 on proliferation of different types of T cells are non-consuming delayed reactions; all other reactions are non-delayed. According to the methodology of Fatehi et al. [58], the order of these reactions in the table is irrelevant, since they all come in with associated state change vectors. The assumption of only a single transition/reaction occurring during a small time interval is a fundamental premise of all stochastic models using the framework of master equation, irrespective of whether they are non-delayed, or delayed, and the same applies to associated stochastic simulations algorithms [52, 54, 96, 88]. Using Table 2 of possible state changes, one can compute the expectation vector and covariance matrix of $\Delta\mathbf{Y}$ for sufficiently small Δt.

The expectation vector to order Δt is now given by

$$\mathbb{E}(\Delta\mathbf{Y}) \approx \sum_{i=1}^{18} P_i(\Delta\mathbf{Y})_i \Delta t = \boldsymbol{\mu}\Delta t,$$

where

$$\boldsymbol{\mu} = \begin{pmatrix} P_1 - P_2 \\ P_3 - P_4 \\ P_5 - P_6 \\ P_7 + P_{10} + P_{11} - P_{12} \\ P_8 + P_{13} - P_{14} \\ P_9 + P_{15} - P_{16} \\ P_{17} - P_{18} \end{pmatrix}$$

is the drift vector, which is identical to the right-hand side of the deterministic model (1). The covariance matrix is obtained by only keeping terms of order Δt, i.e.

$$\mathrm{cov}(\Delta \mathbf{Y}) \approx \sum_{i=1}^{18} P_i (\Delta \mathbf{Y})_i (\Delta \mathbf{Y}_i)^T \Delta t = \Sigma \Delta t,$$

where

$$\Sigma = \begin{pmatrix} P_1 + P_2 & 0 & 0 & 0 & 0 & 0 & 0 \\ 0 & P_3 + P_4 & 0 & 0 & 0 & 0 & 0 \\ 0 & 0 & P_5 + P_6 & 0 & 0 & 0 & 0 \\ 0 & 0 & 0 & P_7 + P_{10} + P_{11} + P_{12} & 0 & 0 & 0 \\ 0 & 0 & 0 & 0 & P_8 + P_{13} + P_{14} & 0 & 0 \\ 0 & 0 & 0 & 0 & 0 & P_9 + P_{15} + P_{16} & 0 \\ 0 & 0 & 0 & 0 & 0 & 0 & P_{17} + P_{18} \end{pmatrix}$$

is a 7×7 diffusion matrix. Since Σ is a diagonal matrix, it is straightforward to find the matrix Q, which is also a diagonal matrix with entries $Q_{ii} = \sqrt{\Sigma_{ii}}$ for $1 \leq i \leq 7$, which satisfies the condition $QQ^T = \Sigma$. The Itô SDDE model is then given by

$$\begin{cases} d\mathbf{Y}(t) = \boldsymbol{\mu} dt + Q d\mathbf{W}(t), \\ \mathbf{Y}(t) = \boldsymbol{\varphi}(t) \quad \text{for} \quad t \in [-\tau, 0], \end{cases} \tag{10}$$

where $\tau = \max\{\tau_1, \tau_2, \tau_3\}$, and $\mathbf{W}(t) = [W_1(t), W_2(t), \ldots, W_7(t)]^T$ is a vector of seven independent Wiener processes, and $\boldsymbol{\varphi}(t)$ is the vector of initial conditions. In the next section we will use this SDDE for numerical simulations to illustrate various dynamical behaviours of the model.

Having now encountered a number of different formulations of the same model, in the Table 1 below, we provide a summary of different modelling approaches along with their strengths and weaknesses.

Table 1: Comparison of different modelling formulations

Method	Strengths	Weaknesses
DDEs	Possibility of analytical results Ease of numerical simulations and bifurcation analyses	Only covers deterministic dynamics
DSSAs	Stochastically exact	Computationally expensive No analytical results
DCMEs	Describes exact probability distribution Serves as a basis for SDDEs	Difficult/impossible to solve analytically
SDDEs	Computationally efficient	An approximation; only works for sufficiently large system size and sufficiently large delays
LNA	Approximates the PDF Allows to determine the variance and coherence of oscillations	An approximation; only works for sufficiently large system sizes, and in close proximity of deterministic solutions

6 Numerical stability analysis and simulations

In order to perform numerical simulations of the model (10), we use the strong predictor-corrector method with the degree of implicitness in the drift coefficient chosen to be equal to 1/7, since for this value the method has the largest stability region [97, 98]. It has been previously shown [47, 48] that in the model (1), the disease-free steady state S_1^* undergoes a transcritical bifurcation at $\beta N = d_F$, where β is the infection rate, N is the carrying capacity of uninfected cells, and d_F is the natural death rate of infected cells. For $\beta N < d_F$, the disease-free steady state is stable, while the chronic infection steady state S_4^* is infeasible. On the contrary, for $\beta N > d_F$, the disease-free steady state is unstable, and in this case we can study the stability of the chronic infection steady

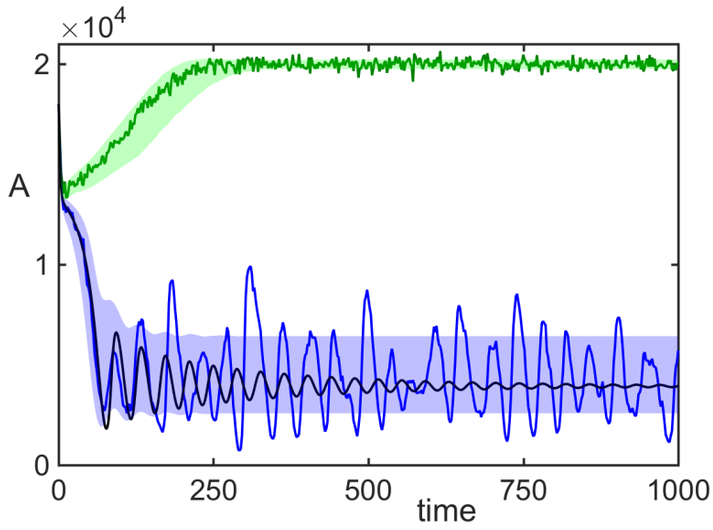

Figure 3: Numerical simulation of the model (10) with parameter values from Table 3, with $\mu_a = 2$, where μ_a is the removal rate of uninfected cells by autoreactive T cells, $x_2(0) = 2$ with a constant history, and the initial condition (11). Blue and green curves represent two sample trajectories of the SDDE (10) that have entered the basins of attraction of steady states S_3^* and S_1^*, respectively. Shaded areas around them them indicate regions of one standard deviation from the mean of 20000 simulations. Black curve is the deterministic trajectory of the DDE model (1).

state [47, 48]. This qualitative distinction between different regimes suggests that it is feasible to consider the two cases separately. First, we consider a situation corresponding to the parameter regime $\beta N < d_F$, with the values of parameters given in Table 3 in **Appendix E** [46, 96]. The initial condition is chosen to be

$$\begin{aligned} &(x_1(s), x_3(s), x_4(s), x_5(s), x_6(s), x_7(s)) = (18, 7.2, 6.3, 0, 0, 0), \\ &s \in [-\tau_{max}, 0], \quad \tau_{max} = \max\{\tau_1, \tau_2, \tau_3\}, \end{aligned} \tag{11}$$

to model a situation at the start of infection, where there is some positive number of infected cells F, but there are still no regulatory, normal or activated T cells that have emerged through activation of naïve/inactive T cells.

Figure 3 shows the result of 20000 simulations with the initial condition (11) and $x_2(0) = 2$ and $\mu_a = 2$, where μ_a is the removal rate of uninfected cells by autoreactive T cells. In this case, in the deterministic model (1) the steady states S_1^* and S_3^* are both stable, but based on the chosen initial condition, the system is deterministically in the attraction basin of S_3^*. This figure also shows single stochastic trajectories around S_1^* and S_3^*, as well as areas of one standard deviation from the mean in the basins of attraction of these steady states (computed from averaging 20000 simulations), in which trajectories show sustained stochastic oscillations [99, 100]. Taking an average of a large number of simulations that enter the basin of attraction of S_3^* would show a decaying oscillations around S_3^*, which is similar to a deterministic trajectory, while single stochastic trajectories exhibit sustained stochastic oscillations [95, 101]. The reason for this is that at the highest order in the system size, the dynamics of the DCME is captured by the system (1), which is nothing else but the original model (1), and similarly, the main contribution to the SDDE is given by the drift vector that also coincides with the deterministic DDE model, while the diffusion term covers fluctuations around those deterministic trajectories [96, 102]. One should also note that with the system being deterministically the system in the attraction basin of the autoimmune steady state S_3^*, it was still possible for a small number of realisations (around 1.5% of the total number) to successfully clear the infection and reach a disease-free steady state, which corresponds to a spontaneous recovery.

Figure 4(a) illustrates temporal evolution of the probability distribution for the same set of parameters and initial condition as in Fig. 3. The bi-stability between steady states S_1^* and S_3^* results in the system reaching a bimodal stationary distribution after some initial transient, as shown in Fig. 4(b). Increasing the value of the rate μ_a, at which autoreactive T cells are destroying infected and healthy host cells, from 2 to 3.33 shifts dynamical behaviour for the deterministic model (1) to a regime of bi-stability between steady states S_1^* and S_2^*. In this case, with the same initial condition (11) and $x_2(0) = 2.2$, the system is in the basin of attraction of S_2^*. Figures 4(c) and (d) show the evolution of the probability distribution, as well as the final bimodal distribution in this case. Since the size of fluctuations around deterministic solutions scales as $\Omega^{-1/2}$, increasing the size of system Ω would result in the stochastic trajectories being more narrowly centred around deterministic solutions, and, as a result, these bimodal distributions becoming closer to unimodal [92, 102, 103].

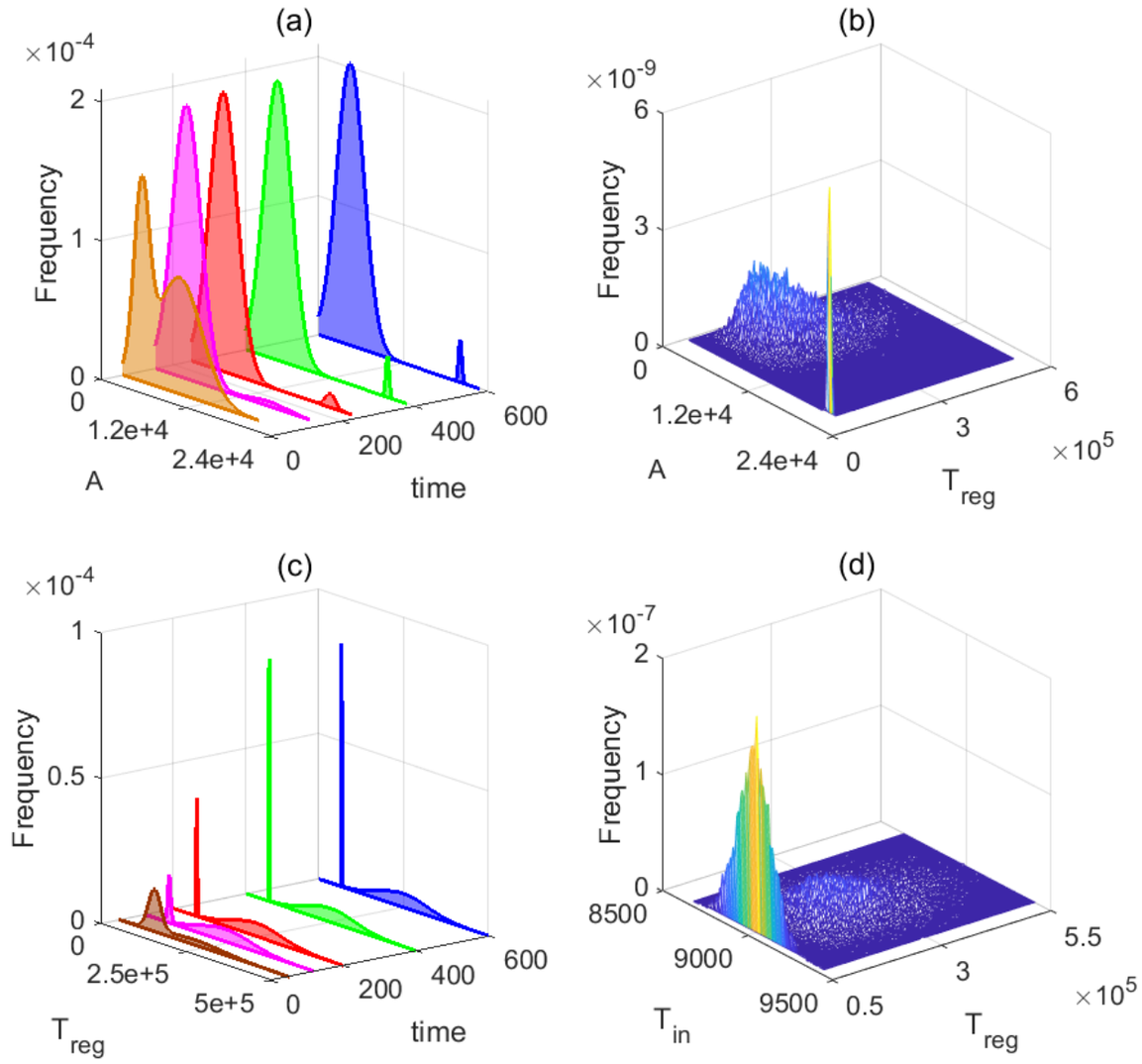

Figure 4: Probability distribution of solutions out of 20000 simulations of the model (10). (a) and (b) with parameters from Table 3 except for $\mu_a = 2$, where μ_a is the removal rate of uninfected cells by autoreactive T cells, and the initial condition (11) with $x_2(0) = 2$ with a constant history. (c) and (d) with parameters from Table 3 except for $\mu_a = 3.33$, and the initial condition (11) with $x_2(0) = 2.2$. In (a) and (c), the probability histogram is fit to a bimodal normal distribution at different times. (b) and (d) illustrate stationary joint probability histograms.

A recent work by Fatehi et al. [46] explored how the basins of attraction of steady states S_1^*, S_2^* and S_3^* (or periodic orbits around around them) are affected by stochasticity. It showed how in the regime of bi-stability, where deterministically depending on the initial conditions for the numbers of infected cells and regulatory T cells, the system is in the basin of attraction of one of those steady states or associated periodic orbits, under the influence of stochasticity the deterministic boundary separating basins of attraction of these different states is smeared out, and for any initial conditions there is some positive probability or reaching either of the states. In contrast, time delays were shown not to have a major effect on changing the boundaries of basins of attraction, besides switching stable steady states into periodic orbits around those steady states [44, 47].

Figure 5 highlights the main difference between deterministic and stochastic models by illustrating how the coherence of stochastic oscillations changes in the region where S_2^* and S_3^* are deterministically stable, i.e. the deterministic solution exhibits damped oscillations that eventually reach a steady state. This figure indicates that by increasing time delay τ_2 associated with the effects of IL-2 on proliferation of T cells, we approach the boundary of the Hopf bifurcation, and the coherence also increases, while in the region where deterministically the model has a periodic solution around these steady states, the value of coherence is equal to one. Biologically, this means that in the parameter region where deterministically the system exhibits damped oscillations, due to stochasticity there would be stochastic oscillations, and they would be becoming more coherent, i.e. having a frequency spectrum more narrowly distributed around the leading frequency, when parameters approach the deterministic stability boundary.

Using equation (9), we can determine the covariance matrix C, which provides the variance of individual state variables, when the deterministic model is at one of its steady states. Figure 6 illustrates how variance in the number of regulatory T cells T_{reg}, as determined by $C_{4,4}$, varies with system parameters in the parameter regions where S_3^* is deterministically stable. One can observe

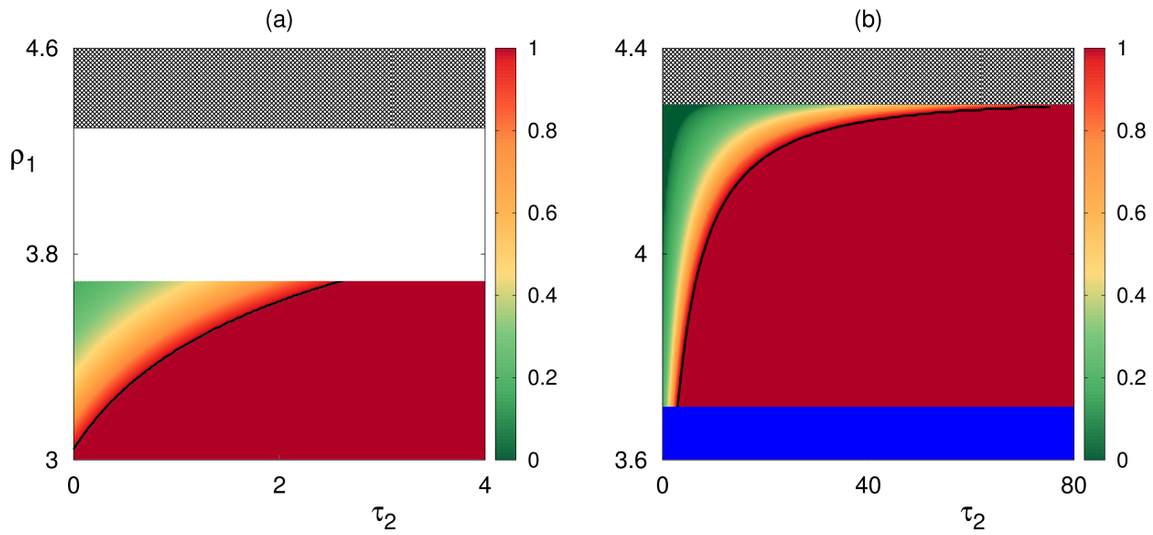

Figure 5: Coherence of oscillations in the stability regions of S_2^* (a) and S_3^* (b) with parameter values from Table 3, except for $\rho_3 = 0.667$, where ρ_3 is the proliferation rate of autoreactive T cells by IL-2. Black curves show deterministic boundaries of Hopf bifurcation for respective steady states. In the white region, the steady state S_2^* is infeasible, in the blue region the steady state S_3^* is infeasible, and in the region indicated by the black grid both steady states S_2^* and S_3^* are infeasible.

that as one gets closer to the border between the area, where S_3^* is stable, and the area, where the deterministic model can have a periodic solution around S_3^*, the variance of stochastic oscillations in Tregs increases. Moreover, this variance increases with the rate σ_2 of production of IL-2 by autoreactive T cells, as well as with the time delay τ_2 associated with stimulation and proliferation of T cells by IL-2. In contrast, Figure 6(b) suggests that the variance of stochastic oscillations in Tregs is insensitive to changes in the rate μ_a of destruction of infected and healthy host cells by autoreactive T cells. The value of variance shown in this figure coincides with the value of variance computed from the average of 20000 simulations shown in Fig. 3.

To illustrate biological significance of simultaneous presence of time delays and stochasticity, in Fig. 7 we fix the values of all parameters as in Table 3 and explore the role of initial conditions for different values of time delays. In the case where all time delays are equal to zero, deterministically the system approaches a disease-free steady state S_1^* for sufficiently small initial number of infected cells $F(0)$ and/or for sufficiently large initial number of regulatory T cells $T_{reg}(0)$. Due to stochasticity, the deterministic boundary separating basins of attraction of these two steady states becomes smeared, and there is a non-zero probability that the system will approach either of these steady states on both sides of the deterministic boundary separating their basins of attraction. When time delays are chosen to have the values as given in Table 3, the shape of the region delineating deterministic basins of attraction of these two steady states changes, and it is deterministically possible for the system to approach a disease-free steady state S_3^* even for large initial values of the number of infected cells, provided the initial number of Tregs is sufficiently small. As the time delay τ_2 is increased, this makes the steady state S_3^* lose stability, and Figure 7(c) illustrates a regime of bi-stability between a disease-free steady state S_1^* and a periodic solution around S_3^*, which represents an autoimmune state. In this case, there is a range of initial numbers of infected cells, for which, provided the initial number of Tregs is sufficiently low, the majority of solutions would go to autoimmune state, while a small proportion of them would be able to clear the infection without any lasting consequences. For higher initial numbers of infected cells, this escape to disease clearance (which deterministically is impossible) can only take place provided the initial numbers of Tregs lie in a certain range. Conversely, in the case where deterministically the system would approach a disease-free steady state, there is now a non-zero probability that some proportion of stochastic realisations will go on to develop autoimmunity for the same values of parameters and the same initial conditions.

Now we consider a situation where $\beta N > d_F$, in which case deterministically the disease-free steady state S_1^* is unstable, and we can investigate stability of the chronic steady state S_4^*. Earlier results by Fatehi et al. [47, 48] indicate that for parameter values from Table 3, but with $\delta = 5.3\text{e-}4$, $\sigma_2 = 0.66$ and $\beta = 0.14$, where δ is the clearance rate of autoreactive T cells by regulatory T cells, σ_2 is the production rate of IL-2 by autoreactive T cells, and β is the infection rate, the steady states S_3^* and S_4^* are both deterministically stable, and for the initial condition (11) with $x_2(0) = 0.6$ and $x_4(0) = 36$ with a constant history, the model (1) is in the basin of attraction of the chronic steady state S_4^*.

Figure 8 shows the results of 20000 stochastic simulations with these parameter values and initial conditions. Since deterministically S_4^* is stable, and the system is in its basin of attraction

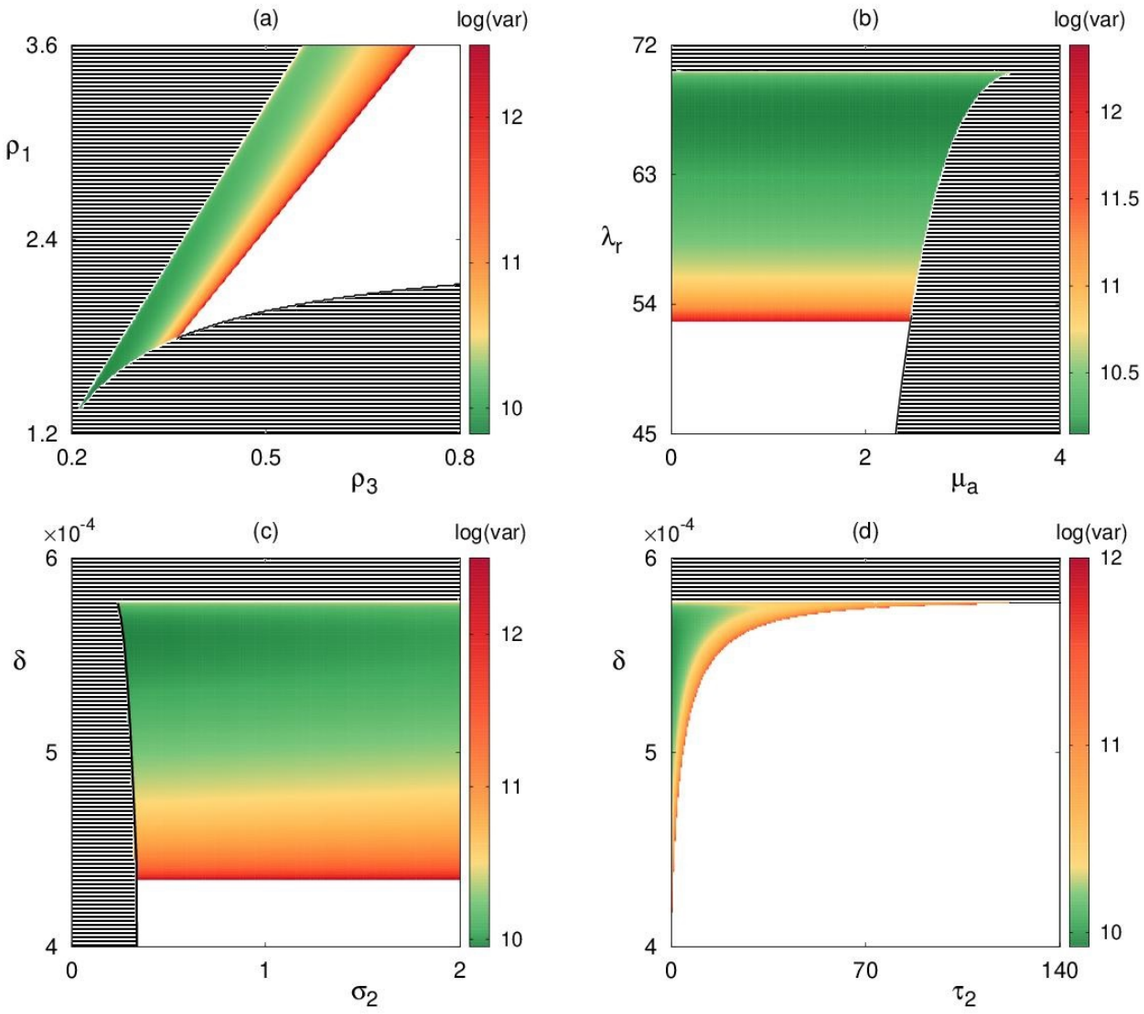

Figure 6: Variance of the number of regulatory T cells with parameter values from Table 3, but $\mu_a = 2$ (removal rate of uninfected cells by autoreactive T cells) using equation (9). Coloured regions indicate areas in respective parameter planes where the autoimmune steady state S_3^* is deterministically stable. Black lined area indicates the region where S_3^* is infeasible, and in the white region it is feasible but unstable.

for the specific chosen initial conditions, the majority of stochastic trajectories also enter the basin of attraction of S_4^*. Due to bi-stability, a proportion of these trajectories (about 17.5%) go to S_3^*. Interestingly, although the disease-free steady state is deterministically unstable, fewer than two percent of trajectories still approach S_1^* and exhibit stochastic oscillations around it. The impact of these trajectories can be observed in Fig. 8(b), which shows temporal evolution of the probability distribution of the solutions. In this figure, initially one observes a trimodal probability distribution, where the middle peak corresponds to trajectories approaching S_1^*. Over time, this peak disappears, while the peak at S_3^* becomes more pronounced. Since the proportion of trajectories going to S_1^* is very small, and the amounts of healthy cells A in the steady states S_4^* and S_1^* are close, the stationary probability distribution is effectively bimodal with peaks at S_3^* and S_4^*. However, the presence of a small number of trajectories approaching the steady state S_1^* results in a small reduction of the peak associated with the chronic steady state S_4^*.

Figure 9 illustrates how the coherence of stochastic oscillations around the chronic steady state S_4^* changes with parameters. We observe that the general trend is similar to that shown earlier in Fig. 5 for steady states S_2^*/S_3^* in that approaching the deterministic boundary of the Hopf bifurcation results in the increase of coherence, while increasing the rate δ at which regulatory T cells suppress autoreactive T cells reduces the coherence of stochastic oscillations. When this rate is very small, the chronic steady state S_4^* is infeasible, and once δ increases past some minimum threshold, the steady state S_4^* becomes feasible but unstable, with a deterministic periodic orbit around it, which corresponds to the maximum level of coherence. Increasing δ further results in stabilisation of the steady state S_4^* and a reduced coherence of stochastic oscillations around the stable steady state. There is a major difference in behaviour with regards to effects of time delays. For the time delay τ_2, associated with stimulation and proliferation of T cells by IL-2, there are multiple stability switches in the stability of S_4^* for intermediate values of δ, which leads to successive growth and reduction in the level of coherence. In contrast, increasing time delay τ_3, which characterises a lag in proliferation and differentiation of naïve T cells, there is a single stability switch, with coherence being low for small values of this time delay, then increasing all the

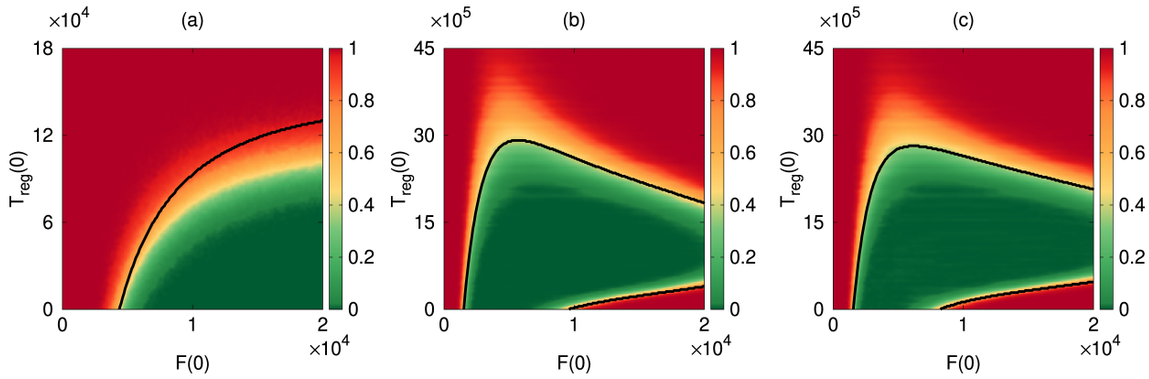

Figure 7: Probability of solution entering and staying in the basin of attraction of the disease-free steady state S_1^*. Black curves indicate boundaries between different basins of attraction in the deterministic model, with parameter values from Table 3, except for $\tau_i = 0$ (a), all delays as in Table 3 (b) and (c), except for $\tau_2 = 1$ in (c). (a) and (b) illustrate bi-stability between steady states S_1^* and S_3^*, (c) shows the regime of bi-stability between a stable steady state S_1^* and a periodic solution around the autoimmune steady state S_3^*.

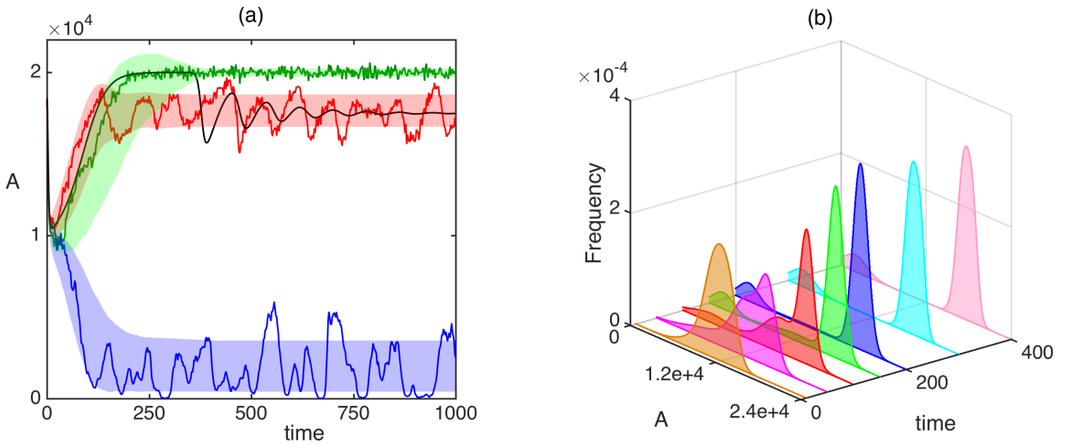

Figure 8: (a) Numerical simulations and (b) probability distribution out of 20000 simulations of the model (10) with parameter values from Table 3, except for δ = 5.3e-4, $\sigma_2 = 0.66$ and $\beta = 0.14$, where δ is the clearance rate of autoreactive T cells by regulatory T cells, σ_2 is the production rate of IL-2 by autoreactive T cells, and β is the infection rate, and the initial condition (11) with $x_2(0) = 0.6$ and $x_4(0) = 36$ with a constant history. In (a) blue, red and green are sample trajectories, which have entered the basins of attraction of S_1^*, S_4^* and S_3^*, respectively. Black curve is the deterministic trajectory of the model (1), and the shaded areas indicate the regions of one standard deviation from the mean. In (b) the probability histogram is fit to a multimodal normal distribution at different times.

way up to the boundary of Hopf bifurcation, and being at its maximum value subsequently. From a biological perspective, these results indicate that in the parameter region, where the chronic steady state is feasible and stable, as regulatory T cells become more effective in suppressing autoreactive T cells (higher δ), this results in stochastic oscillations around the chronic steady state becoming less regular, and for sufficiently high values of δ, low-coherence stochastic oscillations are observed for arbitrarily large values of time delays τ_2 and τ_3.

In Fig. 10 we illustrate how the variance in the number of regulatory T cells T_{reg} for the steady states S_3^* or S_4^* changes with parameters in the region where these states are deterministically stable. One observes some notable differences in the behaviour of variance for these two steady states. For example, while for the steady state S_3^* the variance appears to be almost completely independent on the rate μ_a, at which autoreative T cells are destroying healthy host cells, for the steady state S_4^* the variance substantially decreases with the increase of this rate. Also, due to the difference in that there is a single loss of stability of S_3^* depending on the time delay τ_2 compared to several stability switches for S_4^*, one observes a monotonic increase of variance for increasing values of τ_2 for S_3^*, whereas in the case of S_4^*, periods of increased variance are followed by periods of decreased variance until it settles on some steady level.

7 Discussion

In this paper we have analysed stochastic aspects of immune response against a viral infection with account for T cells with different activation thresholds, regulatory T cells, as well as the cytokine mediating T cell activity, while paying particular attention to viral and cytokine delays. Using the

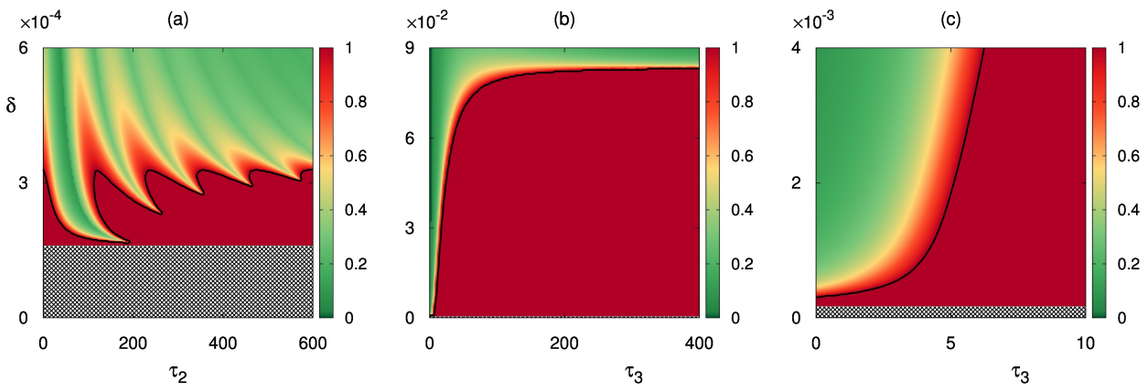

Figure 9: Coherence of oscillations in the region of stability of S_4^* with parameters from Table 3, except for $\sigma_2 = 0.66$ (production rate of IL-2 by autoreactive T cells) and $\beta = 0.14$ (infection rate). Black curves show the deterministic boundary of Hopf bifurcation. The steady state S_4^* is infeasible in the region indicated with a black grid.

framework of delayed chemical reactions, we have carefully reinterpreted various transitions and interactions in the model as discrete stochastic changes in the populations of state variables to derive a delayed chemical master equation that describes the dynamics of the probability distribution of finding the system in a particular state. To make further progress, we used the formalism of consuming and non-consuming delayed reactions to reformulate the DCME as an SDDE. We have proven the equivalence between different formulations of the resulting SDDE, which are identical in terms of probability distribution and sample paths. Using this equivalence, we have proposed an alternative formulation of the SDDE, which is much more amenable to direct numerical treatment. Applying system size expansion to the exact DCME, we have derived a linear Langevin model for our system that characterises stochastic fluctuations around deterministic trajectories, and used this information to derive expressions for the variance of stochastic fluctuations around deterministically stable steady states.

Numerical simulations of the model indicate an intricate interplay between bi-stability and stochasticity. While deterministically the system can be in a basin of attraction of one particular steady state for a chosen combination of parameters, due to stochasticity it rather has a bi-modal probability density distribution, with a proportion of trajectories approaching another stable steady state. We have illustrated this feature by exploring stochastic basins of attraction of different steady states and periodic orbits depending on time delays. Moreover, we have observed that in a small number of realisations, solutions trajectories may exhibit oscillations around the disease-free steady state, which itself is unstable, and the system possesses a stable chronic steady state, suggesting theoretical possibility of a spontaneous clearance of infection. The reason for this is that, as is clear from the Table 2, the disease-free state is an absorbing state of the stochastic model, and thus, provided this model is run for long enough, the solutions would reach the disease-free state state and they stay there. However, since we are only performing simulations over a limited time interval, we rather observe a quasi-stationary distribution [104]. The effect of time delays consists in possibly destabilising some of the steady states, and in each case the computations indicate that the variance of stochastic oscillations around deterministically stable steady states increases as one approaches the stability boundary from the stable side. We have also observed that some parameters may have almost no effect on the variance of oscillations around one steady state, while having a significant effect on the variance of oscillations around another steady state for all other values of parameters being the same. Increasing the rates of homeostatic production of regulatory T cells λ_r or the rate of suppression of autoreactive T cells by regulatory T cells δ results in the reduction of variance of oscillations.

An important practical observation concerns the difference between mean, or averaged, dynamics and the behaviour of individual stochastic realisations [46]. Even in the case when deterministically, or as a result of averaging of a large number of simulations, the system can be settling on a stable steady state, individual realisations can still exhibit sustained stochastic oscillations around that steady state. Since the normal laboratory or clinical practice deals with single observations of individual patients, this result suggests the importance of properly accounting for stochastic effects when developing realistic models of immune dynamics. Numerical simulations of the SDDE model have illustrated the behaviour of individual stochastic trajectories, as well as the time evolution of the probability distribution of the solutions.

There are a number of interesting potential extensions of this work. In terms of more accurate representation of immune response, one could consider including in the model the effects of regulatory T cells on controlling IL-2 secretion [47, 22], as well as memory T cells [105, 106]. A

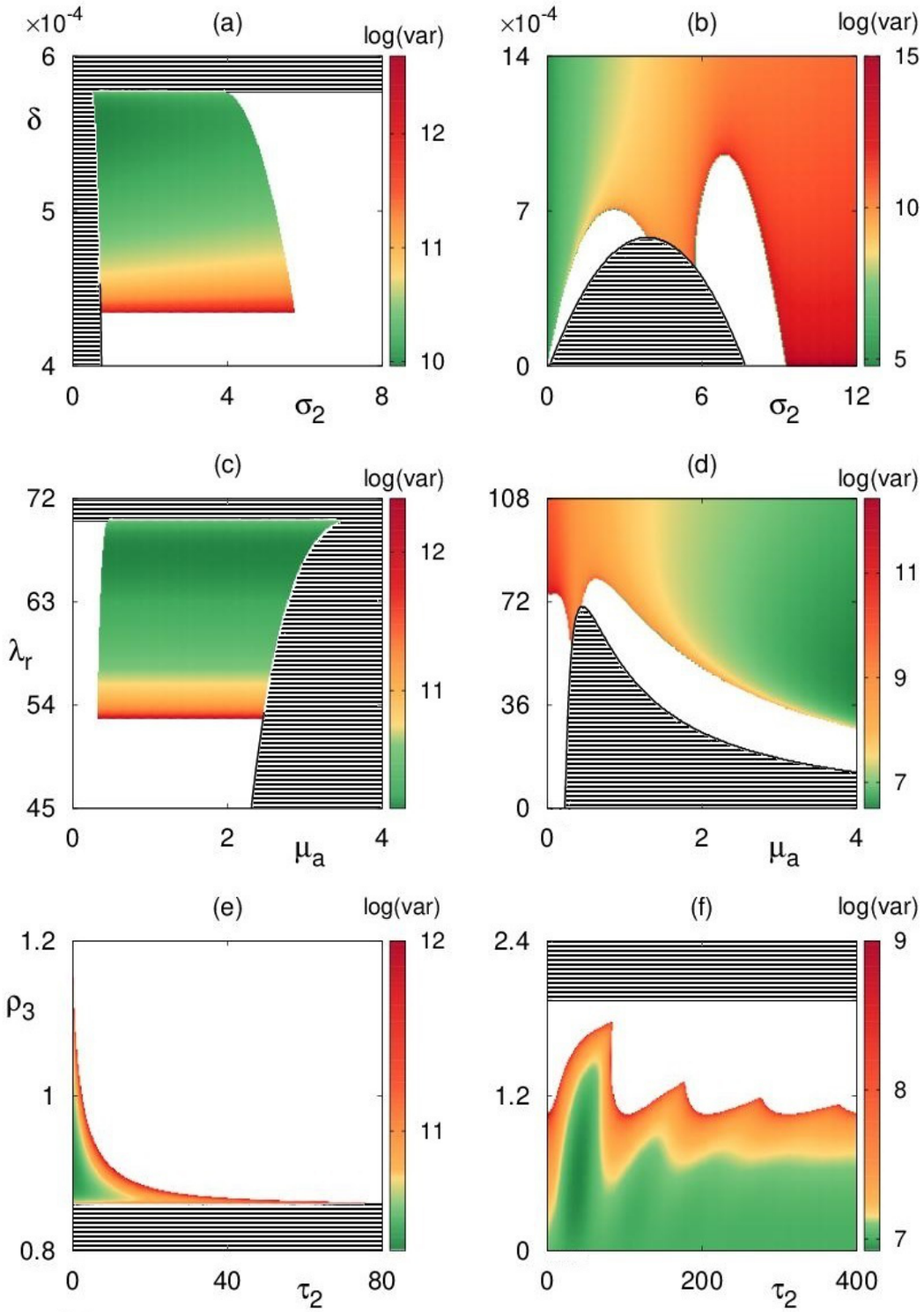

Figure 10: Variance of the number of regulatory T cells with parameter values from Table 3 and $\beta = 0.14$ (infection rate), but in (e) and (f) $\rho_1 = 5.55$ (proliferation rate of regulatory T cells by IL-2) using equation (9). In the left (respectively, right) column, coloured regions indicate areas of respective parameter planes where the autoimmune (respectively, chronic) steady state S_3^* (respectively, S_4^*) is deterministically stable, white areas are regions where the steady state is feasible but unstable, and the black lined area indicates the region where the steady state is infeasible.

related question to explore concern the role of other cytokines, such as IL-7 [107], TGF-β and IL-10 [73], which are also known to have a significant impact on proliferation of different T cells and mediating their efficiency in eliminating the infection. Including different cytokines can provide a better insight into the dynamics of immune response, as has been recently shown in a detailed model of immune response to hepatitis B [108]. A number of papers have considered time-delayed stochastic models of cellular processes that also explicitly include cell division, but from a perspective of direct stochastic simulation [109, 110, 111, 112]. While in the current model, the dynamics of uninfected cells is described by logistic growth, it would be interesting to explore how one could include cell division as an alternative and more realistic representation for the dynamics of cell populations within the framework of SDDEs.

Having computed the variance of stochastic oscillations depending on parameters, it would

interesting and insightful to compare these results to experimental data on the progress and variation of autoimmune disease. One possibility for such a comparison is provided by the recent work on experimental autoimmune uveoretinitis (EAU), where it has been observed that in genetically identical C57BL/6 mice, once the EAU was induced in them through inoculation, the autoimmune disease then progressed at slightly different rates [113]. At the same time, in order to be able to perform such a comparison even at a qualitative level, it is essential to first verify that the main underlying immunological assumptions of the model hold for the particular experimental systems being considered, which itself is a challenge from the perspective of being able to measure a significant number of parameters and cell populations. In this respect, comparing theoretical estimates of the variance in this model with the measured variability in the numbers of T cells and infected cells could provide really important insights and validation of the approach developed in this paper.

Appendix A: Table of propensity functions

Propensity functions corresponding to interactions and transitions between cell populations illustrated in Fig. 1 and described in deterministic model (1), together with associated state change vectors, are given by

$$a_j(\mathbf{X}) = \begin{cases} sX_1, & \mathbf{v}_1 = (1,0,0,0,0,0,0), \\ X_1\left(sX_1/N + \mu_a X_6\right), & \mathbf{v}_2 = (-1,0,0,0,0,0,0), \\ \beta X_1 X_2, & \mathbf{v}_3 = (-1,1,0,0,0,0,0), \\ X_2\left(d_F + \mu_F X_5 + \mu_a X_6\right), & \mathbf{v}_4 = (0,-1,0,0,0,0,0), \\ \lambda_{in}, & \mathbf{v}_5 = (0,0,1,0,0,0,0), \\ d_{in} X_3, & \mathbf{v}_6 = (0,0,-1,0,0,0,0), \\ p_1\alpha X_2 X_3, & \mathbf{v}_7 = (0,0,-1,1,0,0,0), \\ p_2\alpha X_2 X_3, & \mathbf{v}_8 = (0,0,-1,0,1,0,0), \\ (1-p_1-p_2)\alpha X_2 X_3, & \mathbf{v}_9 = (0,0,-1,0,0,1,0), \\ \lambda_r, & \mathbf{v}_{10} = (0,0,0,1,0,0,0), \\ \rho_1 X_4 X_7, & \mathbf{v}_{11} = (0,0,0,1,0,0,0), \\ d_r X_4, & \mathbf{v}_{12} = (0,0,0,-1,0,0,0), \\ \rho_2 X_5 X_7, & \mathbf{v}_{13} = (0,0,0,0,1,0,0), \\ d_n X_5, & \mathbf{v}_{14} = (0,0,0,0,-1,0,0), \\ \rho_3 X_6 X_7, & \mathbf{v}_{15} = (0,0,0,0,0,1,0), \\ X_6\left(d_a + \delta X_4\right), & \mathbf{v}_{16} = (0,0,0,0,0,-1,0), \\ \sigma_1 X_5 + \sigma_2 X_6, & \mathbf{v}_{17} = (0,0,0,0,0,0,1), \\ d_i X_7, & \mathbf{v}_{18} = (0,0,0,0,0,0,-1). \end{cases} \tag{12}$$

Appendix B: System-size expansion of propensity functions

Non-delayed reactions:

$$\begin{aligned} a_2(\mathbf{n}) + a_3(\mathbf{n}) =& d_2\xi_1^2 + \mu_a\xi_1\xi_6 + \beta\xi_1\xi_2 + (2d_2x_1\xi_1 + \mu_a x_1\xi_6 + \mu_a x_6\xi_1 + \beta x_1\xi_2 + \beta x_2\xi_1)\Omega^{1/2} \\ &+ \left(d_2x_1^2 + \mu_a x_1x_6 + \beta x_1x_2\right)\Omega, \end{aligned}$$

$$\begin{aligned} a_4(\mathbf{n}) =& \mu_F\xi_2\xi_5 + \mu_a\xi_2\xi_6 + (d_F\xi_2 + \mu_F x_2\xi_5 + \mu_F x_5\xi_2 + \mu_a x_2\xi_6 + \mu_a x_6\xi_2)\Omega^{1/2} \\ &+ (d_F x_2 + \mu_F x_2x_5 + \mu_a x_2x_6)\Omega, \end{aligned}$$

$$a_5(\mathbf{n}) = \lambda_{in}\Omega, \quad a_{10}(\mathbf{n}) = \lambda_r\Omega, \quad a_{12}(\mathbf{n}) = d_r\xi_4\Omega^{1/2} + d_r x_4\Omega, \quad a_{14}(\mathbf{n}) = d_n\xi_5\Omega^{1/2} + d_n x_5\Omega,$$

$$a_6(\mathbf{n}) + a_7(\mathbf{n}) + a_8(\mathbf{n}) + a_9(\mathbf{n}) = \alpha\xi_2\xi_3 + (d_{in}\xi_3 + \alpha x_2\xi_3 + \alpha x_3\xi_2)\Omega^{1/2} + (d_{in}x_3 + \alpha x_2x_3)\Omega,$$

$$a_{16}(\mathbf{n}) = \delta\xi_4\xi_6 + (d_a\xi_6 + \delta x_4\xi_6 + \delta x_6\xi_4)\Omega^{1/2} + (d_a x_6 + \delta x_4 x_6)\Omega,$$

$$a_{17}(\mathbf{n}) = (\sigma_1\xi_5 + \sigma_2\xi_6)\Omega^{1/2} + (\sigma_1 x_5 + \sigma_2 x_6)\Omega, \quad a_{18}(\mathbf{n}) = d_i\xi_7\Omega^{1/2} + d_i x_7\Omega.$$

Delayed reactions:

$$a_3(\mathbf{m}) = \beta\eta_1\eta_2 + \big(\beta x_1(t-\tau_1)\eta_2 + \beta x_2(t-\tau_1)\eta_1\big)\Omega^{1/2} + \beta x_1(t-\tau_1)x_2(t-\tau_1)\Omega.$$

$$a_8(\mathbf{m}) = p_2\alpha\eta_2\eta_3 + \big(p_2\alpha x_2(t-\tau_3)\eta_3 + p_2\alpha x_3(t-\tau_3)\eta_2\big)\Omega^{1/2} + p_2\alpha x_2(t-\tau_3)x_3(t-\tau_3)\Omega,$$

$$\begin{aligned} a_9(\mathbf{m}) =& (1-p_1-p_2)\alpha\eta_2\eta_3 + (1-p_1-p_2)\big(\alpha x_2(t-\tau_3)\eta_3 + \alpha x_3(t-\tau_3)\eta_2\big)\Omega^{1/2} \\ &+ (1-p_1-p_2)\alpha x_2(t-\tau_3)x_3(t-\tau_3)\Omega, \end{aligned}$$

$$a_{11}(\mathbf{m}) = \rho_1\eta_4\eta_7 + \big(\rho_1 x_4(t-\tau_2)\eta_7 + \rho_1 x_7(t-\tau_2)\eta_4\big)\Omega^{1/2} + \rho_1 x_4(t-\tau_2)x_7(t-\tau_2)\Omega,$$

$$a_{13}(\mathbf{m}) = \rho_2\eta_5\eta_7 + \big(\rho_2 x_5(t-\tau_2)\eta_7 + \rho_2 x_7(t-\tau_2)\eta_5\big)\Omega^{1/2} + \rho_2 x_5(t-\tau_2)x_7(t-\tau_2)\Omega,$$

$$a_{15}(\mathbf{m}) = \rho_3\eta_6\eta_7 + \big(\rho_3 x_6(t-\tau_2)\eta_7 + \rho_3 x_7(t-\tau_2)\eta_6\big)\Omega^{1/2} + \rho_3 x_6(t-\tau_2)x_7(t-\tau_2)\Omega.$$

Appendix C: Delayed Fokker-Planck equation (linear-noise approximation)

$$\begin{aligned} \frac{\partial\Pi}{\partial t} =& -\frac{\partial}{\partial\xi_1}\big[(s\xi_1 - 2d_2x_1\xi_1 - \mu_a x_1\xi_6 - \mu_a x_6\xi_1 - \beta x_1\xi_2 - \beta x_2\xi_1)\Pi\big] \\ &- \frac{\partial}{\partial\xi_2}\big[-(d_F\xi_2 + \mu_F x_2\xi_5 + \mu_F x_5\xi_2 + \mu_a x_2\xi_6 + \mu_a x_6\xi_2)\Pi\big] \\ &- \frac{\partial}{\partial\xi_2}\int_{\boldsymbol{\eta}}\big(\beta x_1(t-\tau_1)\eta_2 + \beta x_2(t-\tau_1)\eta_1\big)\Pi(\boldsymbol{\xi},t;\boldsymbol{\eta},t-\tau_1)d\boldsymbol{\eta} - \frac{\partial}{\partial\xi_3}\big[-(d_{in}\xi_3 + \alpha x_2\xi_3 + \alpha x_3\xi_2)\Pi\big] \\ &- \frac{\partial}{\partial\xi_4}(-d_r\xi_4\Pi) - \frac{\partial}{\partial\xi_4}\int_{\boldsymbol{\eta}}\big(\rho_1 x_4(t-\tau_2)\eta_7 + \rho_1 x_7(t-\tau_2)\eta_4\big)\Pi(\boldsymbol{\xi},t;\boldsymbol{\eta},t-\tau_2)d\boldsymbol{\eta} \\ &- \frac{\partial}{\partial\xi_4}\int_{\boldsymbol{\eta}}\big(p_1\alpha x_2(t-\tau_3)\eta_3 + p_1\alpha x_3(t-\tau_3)\eta_2\big)\Pi(\boldsymbol{\xi},t;\boldsymbol{\eta},t-\tau_3)d\boldsymbol{\eta} \\ &- \frac{\partial}{\partial\xi_5}(-d_n\xi_5\Pi) - \frac{\partial}{\partial\xi_5}\int_{\boldsymbol{\eta}}\big(\rho_2 x_5(t-\tau_2)\eta_7 + \rho_2 x_7(t-\tau_2)\eta_5\big)\Pi(\boldsymbol{\xi},t;\boldsymbol{\eta},t-\tau_2)d\boldsymbol{\eta} \\ &- \frac{\partial}{\partial\xi_5}\int_{\boldsymbol{\eta}}\big(p_2\alpha x_2(t-\tau_3)\eta_3 + p_2\alpha x_3(t-\tau_3)\eta_2\big)\Pi(\boldsymbol{\xi},t;\boldsymbol{\eta},t-\tau_3)d\boldsymbol{\eta} \\ &- \frac{\partial}{\partial\xi_6}\big[-(d_a\xi_6 + \delta x_4\xi_6 + \delta x_6\xi_4)\Pi\big] - \frac{\partial}{\partial\xi_6}\int_{\boldsymbol{\eta}}\big(\rho_3 x_6(t-\tau_2)\eta_7 + \rho_3 x_7(t-\tau_2)\eta_6\big)\Pi(\boldsymbol{\xi},t;\boldsymbol{\eta},t-\tau_2)d\boldsymbol{\eta} \\ &- \frac{\partial}{\partial\xi_6}\int_{\boldsymbol{\eta}}(1-p_1-p_2)\big(\alpha x_2(t-\tau_3)\eta_3 + \alpha x_3(t-\tau_3)\eta_2\big)\Pi(\boldsymbol{\xi},t;\boldsymbol{\eta},t-\tau_3)d\boldsymbol{\eta} \\ &- \frac{\partial}{\partial\xi_7}\big[(\sigma_1\xi_5 + \sigma_2\xi_6 - d_i\xi_7)\Pi\big] + \frac{1}{2}\Big\{\big(sx_1 + d_2x_1^2 + \mu_a x_1x_6 + \beta x_1x_2\big)\frac{\partial^2\Pi}{\partial\xi_1^2} \\ &+ \big(\beta x_1(t-\tau_1)x_2(t-\tau_1) + d_F x_2 + \mu_F x_2x_5 + \mu_a x_2x_6\big)\frac{\partial^2\Pi}{\partial\xi_2^2} + (\lambda_{in} + d_{in}x_3 + \alpha x_2x_3)\frac{\partial^2\Pi}{\partial\xi_3^2} \\ &+ \big(\lambda_r + d_r x_4 + p_1\alpha x_2(t-\tau_3)x_3(t-\tau_3) + \rho_1 x_4(t-\tau_2)x_7(t-\tau_2)\big)\frac{\partial^2\Pi}{\partial\xi_4^2} \\ &+ \big(d_n x_5 + p_2\alpha x_2(t-\tau_3)x_3(t-\tau_3) + \rho_2 x_5(t-\tau_2)x_7(t-\tau_2)\big)\frac{\partial^2\Pi}{\partial\xi_5^2} \\ &+ \big(d_a x_6 + \delta x_4x_6 + (1-p_1-p_2)\alpha x_2(t-\tau_3)x_3(t-\tau_3) + \rho_3 x_6(t-\tau_2)x_7(t-\tau_2)\big)\frac{\partial^2\Pi}{\partial\xi_6^2} \\ &+ (\sigma_1 x_5 + \sigma_2 x_6 + d_i x_7)\frac{\partial^2\Pi}{\partial\xi_7^2}\Big\}. \end{aligned}$$

Appendix D

Table 2: Possible state changes $\Delta\mathbf{Y}$ during a small time interval Δt

i	$(\Delta\mathbf{Y})_i^T$	Probability $P_i\Delta t$
1	$(1,0,0,0,0,0,0)$	$sY_1(t)\Delta t$
2	$(-1,0,0,0,0,0,0)$	$\left(d_2Y_1(t)^2+\mu_aY_6(t)Y_1(t)+\beta Y_1(t)Y_2(t)\right)\Delta t$
3	$(0,1,0,0,0,0,0)$	$\beta Y_1(t-\tau_1)Y_2(t-\tau_1)\Delta t$
4	$(0,-1,0,0,0,0,0)$	$\left[d_F+\mu_FY_5(t)+\mu_aY_6(t)\right]Y_2(t)\Delta t$
5	$(0,0,1,0,0,0,0)$	$\lambda_{in}\Delta t$
6	$(0,0,-1,0,0,0,0)$	$\left[d_{in}Y_3(t)+\alpha Y_3(t)Y_2(t)\right]\Delta t$
7	$(0,0,0,1,0,0,0)$	$p_1\alpha Y_3(t-\tau_3)Y_2(t-\tau_3)\Delta t$
8	$(0,0,0,0,1,0,0)$	$p_2\alpha Y_3(t-\tau_3)Y_2(t-\tau_3)\Delta t$
9	$(0,0,0,0,0,1,0)$	$(1-p_1-p_2)\alpha Y_3(t-\tau_3)Y_2(t-\tau_3)\Delta t$
10	$(0,0,0,1,0,0,0)$	$\lambda_r\Delta t$
11	$(0,0,0,1,0,0,0)$	$\rho_1Y_7(t-\tau_2)Y_4(t-\tau_2)\Delta t$
12	$(0,0,0,-1,0,0,0)$	$d_rY_4(t)\Delta t$
13	$(0,0,0,0,1,0,0)$	$\rho_2Y_7(t-\tau_2)Y_5(t-\tau_2)\Delta t$
14	$(0,0,0,0,-1,0,0)$	$d_nY_5(t)\Delta t$
15	$(0,0,0,0,0,1,0)$	$\rho_3Y_7(t-\tau_2)Y_6(t-\tau_2)\Delta t$
16	$(0,0,0,0,0,-1,0)$	$\left[d_a+\delta Y_4(t)\right]Y_6(t)\Delta t$
17	$(0,0,0,0,0,0,1)$	$\left[\sigma_1Y_5(t)+\sigma_2Y_6(t)\right]\Delta t$
18	$(0,0,0,0,0,0,-1)$	$d_iY_7(t)\Delta t$
19	$(0,0,0,0,0,0,0)$	$1-\sum_{i=1}^{18}P_i\Delta t$

Appendix E

Table 3: Table of parameters

Parameter	Value	Unit	Definition
s	2	day^{-1}	Linear growth rate of uninfected cells
N	20	cell	Carrying capacity of uninfected cells
β	0.1	$\text{cell}^{-1}\text{day}^{-1}$	Infection rate
μ_a	4.44	$\text{cell}^{-1}\text{day}^{-1}$	The rate of killing of uninfected cells by autoreactive T cells
d_a	0.002	day^{-1}	Natural death rate of autoreactive T cells
d_F	2.2	day^{-1}	Natural death rate of infected cells
δ	4.4e-4	$\text{cell}^{-1}\text{day}^{-1}$	Rate of clearance of autoreactive T cells by regulatory T cells
μ_F	1.33	$\text{cell}^{-1}\text{day}^{-1}$	The rate of killing of infected cells by the normal T cells
σ_1	0.3	day^{-1}	Rate of production of IL-2 by normal T cells
σ_2	0.4	day^{-1}	Rate of production of IL-2 by autoreactive T cells
λ_{in}	18	cell day^{-1}	Growth rate of inactive T cells
d_{in}	2	day^{-1}	Natural death rate of inactive T cells
d_i	1.2	day^{-1}	Natural clearance rate of IL-2
α	0.04	$\text{cell}^{-1}\text{day}^{-1}$	Rate of activation of inactive T cells by infected cells
λ_r	54	cell day^{-1}	Growth rate of regulatory T cells
d_r	0.8	day^{-1}	Natural death rate of regulatory T cells
p_1	0.4	–	Proportion of T cells differentiating into regulatory T cells
p_2	0.4	–	Proportion of T cells differentiating into normal T cells
ρ_1	2.22	$\text{cell}^{-1}\text{day}^{-1}$	Proliferation rate of regulatory T cells by IL-2
ρ_2	0.178	$\text{cell}^{-1}\text{day}^{-1}$	Proliferation rate of normal T cells by IL-2
ρ_3	0.44	$\text{cell}^{-1}\text{day}^{-1}$	Proliferation rate of autoreactive T cells by IL-2
d_n	2	day^{-1}	Natural death rate of normal T cells
τ_1	0.7	day	Viral lag
τ_2	0.5	day	Delay in IL-2 enhanced proliferation of T cells
τ_3	0.3	day	Delay in T cell differentiation/expansion
Ω	1000	cell	System size

References

[1] A. K. Abbas, A. H. Lichtman, and S. Pillai, *Cellular and Molecular Immunology*. Elsevier Health Sciences, 2015.

[2] A. Davidson and B. Diamond, "Autoimmune diseases," *N. Engl. J. Med.*, vol. 345, pp. 340–350., 2001.

[3] R. Root-Bernstein and D. Fairweather, "Unresolved issues in theories of autoimmune disease using myocarditis as a framework," *J. Theor. Biol.*, vol. 375, pp. 101–123, 2015.

[4] A. L. P. Caforio and S. Iliceto, "Genetically determined myocarditis: clinical presentation and immunological characteristics," *Curr. Opin. Cardiol.*, vol. 23, no. 3, pp. 219–226, 2008.

[5] H. S. Li, D. L. Ligons, and N. R. Rose, "Genetic complexity of autoimmune myocarditis," *Autoimmun. Rev.*, vol. 7, no. 3, pp. 168–173, 2008.

[6] L. Guilherme, K. F. Köhler, E. Postol, and J. Kalil, "Genes, autoimmunity and pathogenesis of rheumatic heart disease," *Ann. Pediatr. Cardiol.*, vol. 4, no. 1, pp. 13–21, 2011.

[7] M. G. von Herrath and M. B. A. Oldstone, "Virus-induced autoimmune disease," *Curr. Opin. Immunol.*, vol. 8, no. 6, pp. 878–885, 1996.

[8] A. M. Ercolini and S. D. Miller, "The role of infections in autoimmune disease," *Clin. Exp. Immunol.*, vol. 155, no. 1, pp. 1–15, 2009.

[9] M. S. Horwitz, L. M. Bradley, J. Harbetson, T. Krahl, J. Lee, and N. Sarvetnick, "Diabetes induced by Coxsackie virus: initiation by bystander damage and not molecular mimicry," *Nat. Med.*, vol. 4, no. 7, pp. 781–786, 1998.

[10] J. Correale, M. Fiol, and W. Gilmore, "The risk of relapses in multiple sclerosis during systemic infections," *Neurology*, vol. 67, no. 4, pp. 652–659, 2006.

[11] C. Münz, J. D. Lünemann, M. T. Getts, and S. D. Miller, "Antiviral immune responses: triggers of or triggered by autoimmunity?," *Nat. Rev. Immunol.*, vol. 9, no. 4, pp. 246–258, 2009.

[12] R. S. Fujinami, M. G. Von Herrath, U. Christen, and J. L. Whitton, "Molecular mimicry, bystander activation, or viral persistence: infections and autoimmune disease," *Clin. Microbiol. Rev.*, vol. 19, no. 1, pp. 80–94, 2006.

[13] S. Manfredo Vieira, M. Hiltensperger, V. Kumar, D. Zegarra-Ruiz, C. Dehner, N. Khan, *et al.*, "Translocation of a gut pathobiont drives autoimmunity in mice and humans," *Science*, vol. 359, pp. 1156–1161, 2018.

[14] L. A. Segel, E. Jäger, D. Elias, and I. R. Cohen, "A quantitative model of autoimmune disease and T-cell vaccination: does more mean less?," *Immunol. Today*, vol. 16, no. 2, pp. 80–84, 1995.

[15] J. A. M. Borghans and R. J. De Boer, "A minimal model for T-cell vaccination," *Proc. R. Soc. Lond. B Biol. Sci.*, vol. 259, no. 1355, pp. 173–178, 1995.

[16] J. A. M. Borghans, R. J. De Boer, E. Sercarz, and V. Kumar, "T cell vaccination in experimental autoimmune encephalomyelitis: a mathematical model," *J. Immunol.*, vol. 161, no. 3, pp. 1087–1093, 1998.

[17] K. León, R. Perez, A. Lage, and J. Carneiro, "Modelling T-cell-mediated suppression dependent on interactions in multicellular conjugates," *J. Theor. Biol.*, vol. 207, no. 2, pp. 231–254, 2000.

[18] K. León, A. Lage, and J. Carneiro, "Tolerance and immunity in a mathematical model of T-cell mediated suppression," *J. Theor. Biol.*, vol. 225, no. 1, pp. 107–126, 2003.

[19] K. León, J. Faro, A. Lage, and J. Carneiro, "Inverse correlation between the incidences of autoimmune disease and infection predicted by a model of T cell mediated tolerance," *J. Autoimmun.*, vol. 22, no. 1, pp. 31–42, 2004.

[20] J. Carneiro, T. Paixão, D. Milutinovic, J. Sousa, K. Leon, R. Gardner, *et al.*, "Immunological self-tolerance: Lessons from mathematical modeling," *J. Comput. Appl. Math.*, vol. 184, no. 1, pp. 77–100, 2005.

[21] H. K. Alexander and L. M. Wahl, "Self-tolerance and autoimmunity in a regulatory T cell model," *Bull. Math. Biol.*, vol. 73, no. 1, pp. 33–71, 2011.

[22] N. J. Burroughs, B. M. P. M. de Oliveira, and A. A. Pinto, "Regulatory T cell adjustment of quorum growth thresholds and the control of local immune responses," *J. Theor. Biol.*, vol. 241, no. 1, pp. 134–141, 2006.

[23] N. J. Burroughs, M. Ferreira, B. M. P. M. Oliveira, and A. A. Pinto, "A transcritical bifurcation in an immune response model," *J. Diff. Eqns. Appl.*, vol. 17, pp. 1101–1106, 2011.

[24] N. J. Burroughs, M. Ferreira, B. M. P. M. Oliveira, and A. A. Pinto, "Autoimmunity arising from bystander proliferation of T cells in an immune response model," *Math. Comput. Model.*, vol. 53, no. 7, pp. 1389–1393, 2011.

[25] B. M. P. M. Oliveira, R. Trinchet, M. V. O. Espinar, A. Pinto, and N. J. Burroughs, "Modelling the suppression of autoimmunity after pathogen infection," *Math. Meth. Appl. Sci.*, vol. 41, pp. 8565–8570, 2018.

[26] S. Iwami, Y. Takeuchi, Y. Miura, T. Sasaki, and T. Kajiwara, "Dynamical properties of autoimmune disease models: tolerance, flare-up, dormancy," *J. Theor. Biol.*, vol. 246, no. 4, pp. 646–659, 2007.

[27] S. Iwami, Y. Takeuchi, K. Iwamoto, Y. Naruo, and M. Yasukawa, "A mathematical design of vector vaccine against autoimmune disease," *J. Theor. Biol.*, vol. 256, no. 3, pp. 382–392, 2009.

[28] Z. Grossman and W. E. Paul, "Adaptive cellular interactions in the immune system: the tunable activation threshold and the significance of subthreshold responses," *Proc. Natl. Acad. Sci. USA*, vol. 89, no. 21, pp. 10365–10369, 1992.

[29] Z. Grossman and A. Singer, "Tuning of activation thresholds explains flexibility in the selection and development of T cells in the thymus," *Proc. Natl. Acad. Sci. USA*, vol. 93, no. 25, pp. 14747–14752, 1996.

[30] Z. Grossman and W. E. Paul, "Self-tolerance: context dependent tuning of T cell antigen recognition," *Sem. Immunol.*, vol. 12, no. 3, pp. 197–203, 2000.

[31] A. D. Bitmansour, D. C. Douek, V. C. Maino, and L. J. Picker, "Direct *ex vivo* analysis of human $CD4^+$ memory T cell activation requirements at the single clonotype level," *J. Immunol.*, vol. 169, no. 3, pp. 1207–1218, 2002.

[32] L. B. Nicholson, A. C. Anderson, and V. K. Kuchroo, "Tuning T cell activation threshold and effector function with cross-reactive peptide ligands," *Int. Immunol.*, vol. 12, no. 2, pp. 205–213, 2000.

[33] P. S. Römer, S. Berr, E. Avota, S.-Y. Na, M. Battaglia, I. ten Berge, *et al.*, "Preculture of PBMC at high cell density increases sensitivity of T-cell responses, revealing cytokine release by CD28 superagonist TGN1412," *Blood*, vol. 118, no. 26, pp. 6772–6782, 2011.

[34] I. Stefanová, J. R. Dorfman, and R. N. Germain, "Self-recognition promotes the foreign antigen sensitivity of naive T lymphocytes," *Nature*, vol. 420, no. 6914, pp. 429–434, 2002.

[35] A. J. T. George, J. Stark, and C. Chan, "Understanding specificity and sensitivity of T-cell recognition," *Trends Immunol.*, vol. 26, no. 12, pp. 653–659, 2005.

[36] O. Feinerman, R. N. Germain, and G. Altan-Bonnet, "Quantitative challenges in understanding ligand discrimination by $\alpha\beta$T cells," *Mol. Immunol.*, vol. 45, no. 3, pp. 619–631, 2008.

[37] A. Scherer, A. Noest, and R. J. de Boer, "Activation–threshold tuning in an affinity model for the T–cell repertoire," *Proc. R. Soc. Lond. B Biol. Sci.*, vol. 271, no. 1539, pp. 609–616, 2004.

[38] H. A. van den Berg and D. A. Rand, "Dynamics of T cell activation threshold tuning," *J. Theor. Biol.*, vol. 228, no. 3, pp. 397–416, 2004.

[39] K. B. Blyuss and L. B. Nicholson, "The role of tunable activation thresholds in the dynamics of autoimmunity," *J. Theor. Biol.*, vol. 308, pp. 45–55, 2012.

[40] K. B. Blyuss and L. B. Nicholson, "Understanding the roles of activation threshold and infections in the dynamics of autoimmune disease," *J. Theor. Biol.*, vol. 375, pp. 13–20, 2015.

[41] D. Ben Ezra and J. V. Forrester, "Fundal white dots: the spectrum of a similar pathological process," *Brit. J. Ophthalmol.*, vol. 79, no. 9, pp. 856–860, 1995.

[42] T. F. Davies, D. C. Evered, B. Rees Smith, P. P. B. Yeo, F. Clark, and R. Hall, "Value of thyroid-stimulating-antibody determinations in predicting the short-term thyrotoxic relapse in Graves' disease," *Lancet*, vol. 309, no. 8023, pp. 1181–1182, 1977.

[43] A. Nylander and D. A. Hafler, "Multiple sclerosis," *J. Clin. Invest.*, vol. 122, no. 4, pp. 1180–1188, 2012.

[44] F. Fatehi, Y. N. Kyrychko, R. Molchanov, and K. B. Blyuss, "Bifurcations and multi-stability in a model of cytokine-mediated autoimmunity," *Int. J. Bif. Chaos*, vol. 29, p. 1950034, 2019.

[45] A. S. Perelson and G. Weisbuch, "Immunology for physicists," *Rev. Mod. Phys.*, vol. 69, no. 4, pp. 1219–1267, 1997.

[46] F. Fatehi, S. N. Kyrychko, A. Ross, Y. N. Kyrychko, and K. B. Blyuss, "Stochastic effects in autoimmune dynamics," *Front. Physiol.*, vol. 9, p. 45, 2018.

[47] F. Fatehi, Y. N. Kyrychko, and K. B. Blyuss, "Effects of viral and cytokine delays on dynamics of autoimmunity," *Mathematics*, vol. 6, no. 5, p. 66, 2018.

[48] F. Fatehi, Y. N. Kyrychko, and K. B. Blyuss, "Time-delayed model of autoimmune dynamics," *Math. Biosci. Eng.*, vol. 19, pp. 5613–5639, 2019.

[49] D. Bratsun, D. Volfson, L. S. Tsimring, and J. Hasty, "Delay-induced stochastic oscillations in gene regulation," *Proc. Natl. Acad. Sci. USA*, vol. 102, no. 41, pp. 14593–14598, 2005.

[50] M. Barrio, K. Burrage, A. Leier, and T. Tian, "Oscillatory regulation of Hes1: discrete stochastic delay modelling and simulation," *PLoS Comput. Biol.*, vol. 2, no. 9, p. e117, 2006.

[51] D. F. Anderson, "A modified next reaction method for simulating chemical systems with time dependent propensities and delays," *J. Chem. Phys.*, vol. 127, p. 214107, 2007.

[52] X. Cai, "Exact stochastic simulation of coupled chemical reactions with delays," *J. Chem. Phys.*, vol. 126, no. 12, p. 124108, 2007.

[53] A. Leier and T. T. Marquez-Lago, "Delay chemical master equation: direct and closed-form solutions," *Proc. R. Soc. A*, vol. 471, no. 2179, p. 20150049, 2015.

[54] T. Tian, K. Burrage, P. M. Burrage, and M. Carletti, "Stochastic delay differential equations for genetic regulatory networks," *J. Comput. Appl. Math.*, vol. 205, no. 2, pp. 696–707, 2007.

[55] N. E. Phillips, C. S. Manning, T. Pettini, V. Biga, E. Marinopoulou, P. Stanley, *et al.*, "Stochasticity in the miR-9/Hes1 oscillatory network can account for clonal heterogeneity in the timing of differentiation," *Elife*, vol. 5, p. e16118, 2016.

[56] Y. Niu, C. Zhang, and K. Burrage, "Strong predictor-corrector approximation for stochastic delay differential equations," *J. Comput. Math.*, vol. 33, no. 6, pp. 587—605, 2015.

[57] Y. Niu, K. Burrage, and C. Zhang, "Multi-scale approach for simulating time-delay biochemical reaction systems," *IET Syst. Biol.*, vol. 9, no. 1, pp. 31–38, 2015.

[58] F. Fatehi, Y. N. Kyrychko, and K. B. Blyuss, "A new approach to simulating stochastic delayed systems," *Math. Biosci.*, vol. 322, p. 108327, 2020.

[59] P. Baccam, C. Beauchemin, C. A. Macken, F. G. Hayden, and P. A. S, "Kinetics of influenza A virus infection in humans," *J. Virol.*, vol. 80, no. 15, pp. 7590–7599, 2006.

[60] K. A. Pawelek, G. T. Huynh, M. Quinlivan, A. Cullinane, L. Rong, and A. S. Perelson, "Modeling within-host dynamics of influenza virus infection including immune responses," *PLoS Comput. Biol.*, vol. 8, no. 6, p. e1002588, 2012.

[61] M. A. Nowak and R. M. May, *Virus dynamics*. Oxford University Press Oxford, 2000.

[62] S. M. Ciupe, R. M. Ribeiro, P. W. Nelson, G. Dusheiko, and A. S. Perelson, "The role of cells refractory to productive infection in acute hepatitis B viral dynamics," *Proc. Natl. Acad. Sci. USA*, vol. 104, pp. 5050–5055, 2007.

[63] A. Goyal, R. M. Ribeiro, and A. S. Perelson, "The role of infected cell proliferation in the clearance of acute hbv infection in humans," *Viruses*, vol. 9, p. 350, 2017.

[64] P. Krishnapriya and M. Pitchaimani, "Analysis of time delay in viral infection model with immune impairment," *J. Appl. Math. Comput.*, vol. 55, pp. 421–453, 2017.

[65] A. V. M. Herz, S. Bonhoeffer, R. M. Anderson, R. M. May, and M. A. Nowak, "Viral dynamics *in vivo*: limitations on estimates of intracellular delay and virus decay," *Proc. Natl. Acad. Sci. USA*, vol. 93, pp. 7247–7251, 1996.

[66] G. Huang, Y. Takeuchi, and W. Ma, "Lyapunov functionals for delay differential equations model of viral infections," *SIAM J. Appl. Math.*, vol. 70, pp. 2693–2708, 2010.

[67] L. S., S. Ruan, and X. Zhang, "On avian influenza epidemic models with time delay," *Theor. Biosci.*, vol. 134, pp. 75–82, 2015.

[68] C. C. McCluskey and Y. Yang, "Global stability of a diffusive virus dynamics model with general incidence function and time delay," *Nonl. Anal. RWA*, vol. 25, pp. 64–78, 2015.

[69] R. V. Culshaw, S. Ruan, and G. Webb, "A mathematical model of cell-to-cell spread of HIV-1 that includes a time delay," *J. Math. Biol.*, vol. 46, pp. 425–444, 2003.

[70] X. Shi, X. Zhou, and X. Song, "Dynamical behavior of a delay virus dynamics model with CTL immune response," *Nonl. Anal. RWA*, vol. 11, pp. 1795–1809, 2010.

[71] K. A. Pawelek, S. Liu, F. Pahlevani, and L. Rong, "A model of HIV-1 infection with two time delays: Mathematical analysis and comparison with patient data," *Math. Biosci.*, vol. 235, no. 1, pp. 98–109, 2012.

[72] S. D. Wolf, B. N. Dittel, F. Hardardottir, and C. A. Janeway, "Experimental autoimmune encephalomyelitis induction in genetically B cell-deficient mice," *J. Exp. Med.*, vol. 184, no. 6, pp. 2271–2278, 1996.

[73] S. Sakaguchi, "Naturally arising $CD4^+$ regulatory T cells for immunologic self-tolerance and negative control of immune responses," *Ann. Rev. Immunol.*, vol. 22, pp. 531–562, 2004.

[74] C. A. Janeway, P. Travers, M. Walport, and M. J. Shlomchik, *Immunobiology: The Immune System in Health and Disease*. Garland Science, 2005.

[75] I. Baltcheva, L. Codarri, G. Pantaleo, and J.-Y. Le Boudec, "Lifelong dynamics of human $CD4^+CD25^+$ regulatory T cells: Insights from in vivo data and mathematical modeling," *J. Theor. Biol.*, vol. 266, pp. 307–322, 2010.

[76] C. D. Surh and J. Sprent, "Homeostasis of naive and memory T cells," *Nat. Immunol.*, vol. 12, no. 6, pp. 477–484, 2011.

[77] K. Takad and S. C. Jameson, "Naive T cell homeostasis: from awareness of space to a sense of place," *Nat. Rev. Immunol.*, vol. 9, no. 12, pp. 823–832, 2009.

[78] J. Sprent and C. D. Surh, "Normal T cell homeostasis: the conversion of naive cells into memory-phenotype cells," *Nat. Immunol.*, vol. 12, no. 6, pp. 477–484, 2011.

[79] A. R. M. Almeida, N. Legrand, M. Papiernik, and A. A. Freitas, "Homeostasis of peripheral $CD4^+$ T cells: IL-2Rα and IL-2 shape a population of regulatory cells that controls $CD4^+$ T cell numbers," *J. Immunol.*, vol. 169, no. 9, pp. 4850–4860, 2002.

[80] Q. Tang, K. J. Henriksen, E. K. Boden, A. J. Tooley, J. Ye, S. K. Subudhi, X. X. Zheng, T. B. Strom, and J. A. Bluestone, "Cutting edge: CD28 controls peripheral homeostasis of $CD4^+CD25^+$ regulatory T cells," *J. Immunol.*, vol. 171, no. 7, pp. 3348–3352, 2003.

[81] A. M. Thornton and E. M. Shevach, "$CD4^+CD25^+$ immunoregulatory T cells suppress polyclonal T cell activation in vitro by inhibiting interleukin 2 production," *J. Exp. Med.*, vol. 188, pp. 287–296, 1998.

[82] E. M. Shevach, R. S. McHugh, C. A. Piccirillo, and A. M. Thornton, "Control of T-cell activation by $CD4^+CD25^+$ suppressor T cells," *Immunol. Rev.*, vol. 182, pp. 58–67, 2001.

[83] A. Scheffold, K. M. Murphy, and T. Höfer, "Competition for cytokines: T_{reg} cells take all," *Nat. Immunol.*, vol. 8, no. 12, pp. 1285–1287, 2007.

[84] D. Busse, M. de la Rosa, K. Hobiger, K. Thurley, M. Flossdorf, A. Scheffold, and T. Höfer, "Competing feedback loops shape IL-2 signaling between helper and regulatory T lymphocytes in cellular microenvironments," *Proc. Natl. Acad. Sci. USA*, vol. 107, no. 7, pp. 3058–3063, 2010.

[85] D. Kirschner and J. C. Panetta, "Modeling immunotherapy of the tumor-immune interaction," *J. Math. Biol.*, vol. 37, pp. 235–252, 1998.

[86] A. Yates, C. Bergmann, J. L. Van Hemmen, J. Stark, and R. Callard, "Cytokine-mediate regulation of helper T cell populations," *J. Theor. Biol.*, vol. 206, pp. 539–560, 2000.

[87] A. N. Schweitzer and R. M. Anderson, "Dynamic interaction between CD4+ T cells and parasitic helminths: mathematical models of heterogeneity in outcome," *Parasitol.*, vol. 105, pp. 513–522, 1992.

[88] D. T. Gillespie, "The chemical langevin equation," *J. Chem. Phys.*, vol. 113, no. 1, pp. 297–306, 2000.

[89] N. G. van Kampen, *Stochastic processes in physics and chemistry.* Elsevier, 1992.

[90] E. R. Stirk, G. Lythe, H. A. van den Berg, G. A. D. Hurst, and C. Molina-París, "The limiting conditional probability distribution in a stochastic model of T cell repertoire maintenance," *Math. Biosci.*, vol. 224, pp. 74–86, 2010.

[91] E. R. Stirk, G. Lythe, H. A. van den Berg, and C. Molina-París, "Stochastic competitive exclusion in the maintenance of the naïve T cell repertoire," *J. Theor. Biol.*, vol. 265, pp. 396–410, 2010.

[92] T. Galla, "Intrinsic fluctuations in stochastic delay systems: Theoretical description and application to a simple model of gene regulation," *Phys. Rev. E*, vol. 80, no. 2, p. 021909, 2009.

[93] S. Guillouzic, I. L'Heureux, and A. Longtin, "Small delay approximation of stochastic delay differential equations," *Phys. Rev. E*, vol. 59, no. 4, p. 3970, 1999.

[94] J. Pahle, J. D. Challenger, P. Mendes, and A. J. McKane, "Biochemical fluctuations, optimisation and the linear noise approximation," *BMC Syst. Biol.*, vol. 6, p. 86, 2012.

[95] D. Alonso, A. J. McKane, and M. Pascual, "Stochastic amplification in epidemics," *J. R. Soc. Interface*, vol. 4, no. 14, pp. 575–582, 2007.

[96] L. J. S. Allen, *An introduction to stochastic processes with applications to biology.* Chapman and Hall/CRC, 2010.

[97] Y. Niu, K. Burrage, and C. Zhang, "Multi-scale approach for simulating time-delay biochemical reaction systems," *IET Syst. Biol.*, vol. 9, no. 1, pp. 31–38, 2014.

[98] Y. Niu, C. Zhang, and K. Burrage, "Strong predictor-corrector approximation for stochastic delay differential equations," *J. Comput. Math.*, vol. 33, no. 6, pp. 587–605, 2015.

[99] J. M. Conway and D. Coombs, "A stochastic model of latently infected cell reactivation and viral blip generation in treated HIV patients," *PLoS Comput. Biol.*, vol. 7, no. 4, p. e1002033, 2011.

[100] J. Reynolds, M. Coles, G. Lythe, and C. Molina-París, "Deterministic and stochastic naive T cell population dynamics: symmetric and asymmetric cell division," *Dyn. Syst.*, vol. 27, pp. 75–103, 2012.

[101] R. Kuske, L. F. Gordillo, and P. E. Greenwood, "Sustained oscillations via coherence resonance in SIR," *J. Theo. Biol.*, vol. 245, no. 3, pp. 459–469, 2007.

[102] A. J. Black and McKane, "Stochastic formulation of ecological models and their applications," *Trends Ecol. Evol.*, vol. 27, pp. 337–345, 2012.

[103] P. G. Hufton, Y. T. Lin, T. Galla, and A. J. McKane, "Intrinsic noise in systems with switching environments," *Phys. Rev. E*, vol. 93, p. 52119, 2016.

[104] L. J. S. Allen, "An introduction to stochastic epidemic models," in *Mathematical epidemiology* (F. Brauer, P. van den Driessche, and J. Wu, eds.), pp. 81–130, Berlin: Springer, 2008.

[105] A. Skapenko, J. Leipe, P. E. Lipsky, and H. Schulze-Koops, "The role of the T cell in autoimmune inflammation," *Arthr. Res. Ther.*, vol. 7(Suppl 2), pp. S4–S14, 2005.

[106] R. Antia, V. V. Ganusov, and R. Ahmed, "The role of models in understanding $CD8^+$ T-cell memory," *Nature Rev. Immunol.*, vol. 5, no. 2, pp. 101–111, 2005.

[107] K. S. Schluns, W. C. Kieper, S. C. Jameson, and L. Lefrancois, "Interleukin-7 mediates the homeostasis of naïve and memory CD8 T cells *in vivo*," *Nature Immunol.*, vol. 1, pp. 426–432, 2000.

[108] F. Fatehi Chenar, Y. N. Kyrychko, and K. B. Blyuss, "Mathematical model of immune response to hepatitis B," *J. Theor. Biol.*, vol. 447, pp. 98–110, 2018.

[109] L. Chen, R. Wnag, T. Zhou, and K. Aihara, "Noise-induced cooperative behavior in a multicell system," *Bioinf.*, vol. 21, pp. 2722–2729, 2005.

[110] R. Luo, L. Ye, C. Tao, and K. Wang, "Simulation of *E. coli* gene regulation including overlapping cell cycles, growth, division, time delays and noise," *PLoS ONE*, vol. 8, no. 4, p. e62380, 2013.

[111] S. Nakaoka and K. Aihara, "Stochastic simulation of structured skin cell population dynamics," *J. Math. Biol*, vol. 66, pp. 807–835, 2013.

[112] T. R. Maarleveld, B. G. Olivier, and F. J. Bruggeman, "Stochpy: a comprehensive, user-friendly tool for simulating stochastic biological processes," *PLoS ONE*, vol. 8, no. 11, p. e79345, 2013.

[113] J. Boldison, T. K. Khera, D. A. Copland, M. L. Stimpson, G. L. Crawford, A. D. Dick, *et al.*, "A novel pathogenic RBP-3 peptide reveals epitope spreading in persistent experimental autoimmune uveoretinitis," *Immunology*, vol. 146, pp. 301–311, 2015.